

RESEARCH ARTICLE

The glycerol-3-phosphate dehydrogenases GpsA and GlpD constitute the oxidoreductive metabolic linchpin for Lyme disease spirochete host infectivity and persistence in the tick

Dan Drecktrah^{1*}, Laura S. Hall¹, Bethany Crouse^{1^{aa}}, Benjamin Schwarz², Crystal Richards², Eric Bohrsen², Michael Wulf¹, Bonnie Long¹, Jessica Bailey¹, Frank Gherardini², Catharine M. Bosio², Meghan C. Lybecker^{3^{ab}}, D. Scott Samuels^{1,4*}

1 Division of Biological Sciences, University of Montana, Missoula, Montana, United States of America, **2** Laboratory of Bacteriology, National Institute of Allergy and Infectious Diseases, National Institutes of Health, Hamilton, Montana, United States of America, **3** Department of Biology, University of Colorado, Colorado Springs, Colorado, United States of America, **4** Center for Biomolecular Structure and Dynamics, University of Montana, Missoula, Montana, United States of America

^{aa} Current address: Department of Pharmacology, University of Minnesota Medical School, Minneapolis, Minnesota, United States of America

^{ab} Current address: Center for Disease Control and Prevention, Fort Collins, Colorado, United States of America

* dan.drecktrah@mso.umt.edu (DD); samuels@mso.umt.edu (DSS)



OPEN ACCESS

Citation: Drecktrah D, Hall LS, Crouse B, Schwarz B, Richards C, Bohrsen E, et al. (2022) The glycerol-3-phosphate dehydrogenases GpsA and GlpD constitute the oxidoreductive metabolic linchpin for Lyme disease spirochete host infectivity and persistence in the tick. *PLoS Pathog* 18(3): e1010385. <https://doi.org/10.1371/journal.ppat.1010385>

Editor: Jenifer Coburn, Medical College of Wisconsin, UNITED STATES

Received: December 14, 2021

Accepted: February 18, 2022

Published: March 7, 2022

Copyright: This is an open access article, free of all copyright, and may be freely reproduced, distributed, transmitted, modified, built upon, or otherwise used by anyone for any lawful purpose. The work is made available under the [Creative Commons CC0](https://creativecommons.org/licenses/by/4.0/) public domain dedication.

Data Availability Statement: All relevant data are within the manuscript and its [Supporting Information](#) files.

Funding: This work was supported by the National Institute of Allergy and Infectious Diseases of the National Institutes of Health (R01AI130247 to DSS, DD and MCL) and provided by the Division of Intramural Research, National Institute of Allergy and Infectious Diseases of the National Institutes of

Abstract

We have identified GpsA, a predicted glycerol-3-phosphate dehydrogenase, as a virulence factor in the Lyme disease spirochete *Borrelia (Borrelia) burgdorferi*. GpsA is essential for murine infection and crucial for persistence of the spirochete in the tick. *B. burgdorferi* has a limited biosynthetic and metabolic capacity; the linchpin connecting central carbohydrate and lipid metabolism is at the interconversion of glycerol-3-phosphate and dihydroxyacetone phosphate, catalyzed by GpsA and another glycerol-3-phosphate dehydrogenase, GlpD. Using a broad metabolomics approach, we found that GpsA serves as a dominant regulator of NADH and glycerol-3-phosphate levels *in vitro*, metabolic intermediates that reflect the cellular redox potential and serve as a precursor for lipid and lipoprotein biosynthesis, respectively. Additionally, GpsA was required for survival under nutrient stress, regulated overall reductase activity and controlled *B. burgdorferi* morphology *in vitro*. Furthermore, during *in vitro* nutrient stress, both glycerol and *N*-acetylglucosamine were bactericidal to *B. burgdorferi* in a GlpD-dependent manner. This study is also the first to identify a suppressor mutation in *B. burgdorferi*: a *glpD* deletion restored the wild-type phenotype to the pleiotropic *gpsA* mutant, including murine infectivity by needle inoculation at high doses, survival under nutrient stress, morphological changes and the metabolic imbalance of NADH and glycerol-3-phosphate. These results illustrate how basic metabolic functions that are dispensable for *in vitro* growth can be essential for *in vivo* infectivity of *B. burgdorferi* and may serve as attractive therapeutic targets.

Health (CMB and FG). The funders had no role in the study design, data collection and analysis, decision to publish or preparation of the manuscript.

Competing interests: The authors have declared that no competing interests exist.

Author summary

Lyme disease (borreliosis) is the most common tick-borne disease in the Northern hemisphere and its prevalence is increasing. *Borrelia burgdorferi*, the etiological agent of Lyme disease, is an enzootic pathogen that alternates between a tick vector and vertebrate host. Humans are considered an incidental host after transmission of *B. burgdorferi* following the bite of an infected tick. The mechanisms by which *B. burgdorferi* persists in the Ixodid tick, transmits to a vertebrate host and establishes infection are not well understood. Therefore, identifying virulence factors and uncovering the pathogenic strategies in the spirochete remain important to address the public health concerns of Lyme disease. In this study, we identify an enzyme involved in three-carbon metabolism, GpsA, as a new virulence factor with an effect on persistence in ticks. GpsA and GlpD, another enzyme, constitute a bidirectional metabolic node connecting lipid biosynthesis and glycolysis, which serves as the linchpin for regulating carbon utilization for *B. burgdorferi* throughout its enzootic cycle. Disruption of this node causes a lethal metabolic imbalance revealing a potential therapeutic target for the treatment of Lyme disease.

Introduction

Lyme disease is the most prevalent arthropod-borne infection in North America with an estimated 476,000 cases annually in the United States [1]. *Borrelia* (*Borrelia*) *burgdorferi*, the enzootic spirochete that causes Lyme disease [2–4], is maintained in nature by cycling between *Ixodes* ticks and a vertebrate host reservoir, primarily white-footed mice; the bacterium is neither free-living nor transovarially transmitted by the female ticks to oocytes. The reduced genome of *B. burgdorferi* reflects the constraints of host dependence where numerous biosynthetic and energy-producing metabolic pathways have been lost, including amino acid synthesis, nucleotide synthesis, fatty acid synthesis, the citric acid cycle, and the electron transport chain [5,6]. Thus, *B. burgdorferi* has evolved into an unabashed scavenger of amino acids, nucleosides, peptides and various carbon sources including glucose, *N*-acetylglucosamine (GlcNAc) and glycerol. The metabolic capacity retained by *B. burgdorferi* to flourish in the disparate environments of the vertebrate host and tick vector is important to understand as these strategies, in the absence of any identified toxins or secreted effectors, determine survival of the spirochete and thus the pathogenesis of Lyme disease.

Available carbon sources are a dynamic determinant of *B. burgdorferi* persistence and transit through the enzootic cycle [7,8]. Glucose is likely the preferred carbon source of *B. burgdorferi* in the vertebrate host and initially during tick feeding, but other carbohydrates can support growth and have a role during the enzootic cycle [9–11]. In particular, glycerol becomes important for *B. burgdorferi* persistence in the tick as glucose levels decrease when the blood meal is consumed by the tick and its microbiome. This importance is exemplified by the finding that *B. burgdorferi* mutants unable to utilize glycerol for glycolysis are significantly compromised for persistence in the tick, yet remain infectious in the vertebrate host [12–14]. Glycerol also supports *B. burgdorferi* growth *in vitro*, particularly at 23°C, the temperature often used to mimic tick-like conditions [12,13,15]. Glycerol enters the cell through the glycerol uptake facilitator GlpF, is converted to glycerol 3-phosphate (G3P) by the glycerol kinase GlpK and either is shuttled to glycolysis via conversion to dihydroxyacetone phosphate (DHAP) by the glycerol-3-phosphate dehydrogenase (G3PDH) GlpD or serves as the three-carbon backbone for lipid and lipoprotein biosynthesis (Fig 1) [5–7]. The *glp* operon, consisting of the *glpF*, *glpK* and *glpD* genes, along with *bb0242*, is controlled by a diverse repertoire of

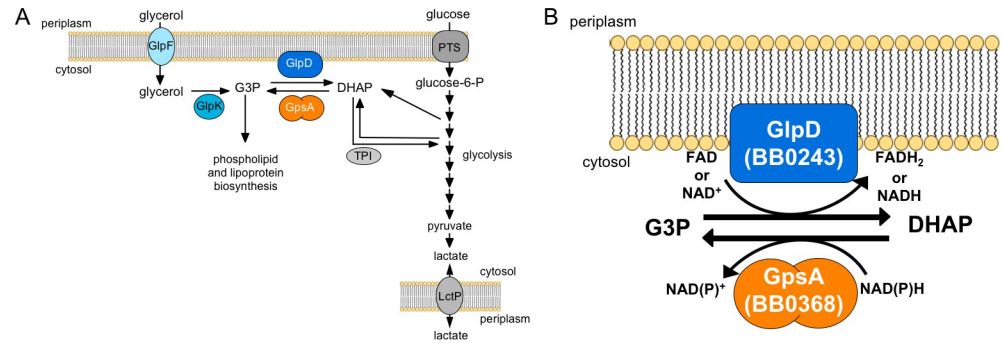


Fig 1. The redox linchpin connecting three-carbon (glycerol) metabolism and six-carbon (glycolysis) metabolism in *B. burgdorferi*. (A) Schematic overview of the intersection of glycerol metabolism and glycolysis, including the conversion of pyruvate to lactate and the use of glycerol-3-phosphate (G3P) for lipid and lipoprotein biosynthesis. Dihydroxyacetone phosphate (DHAP); glycerol uptake facilitator (GlpF, BB0240); glycerol kinase (GlpK, BB0241); glycerol-3-phosphate dehydrogenase (GlpD, BB0243); glycerol-3-phosphate dehydrogenase (GpsA, BB0368); triose phosphate isomerase (TPI); phosphotransferase systems (PTS); lactate permease (LctP). (B) This redox junction consists of two predicted glycerol-3-phosphate dehydrogenases, GlpD and GpsA. GlpD putatively oxidizes G3P to DHAP, while reducing flavin adenine dinucleotide (FAD) or NAD⁺, to feed glycerol into glycolysis. GpsA reduces DHAP to G3P, using the reducing power of NAD(P)H, to provide carbohydrates for lipoproteins and glycerophospholipids.

<https://doi.org/10.1371/journal.ppat.1010385.g001>

regulatory mechanisms [16]. Gene expression is induced during nutrient stress by the stringent response mediated by Rel_{Bbu}, (p)ppGpp and the effector protein DksA [15,17,18], by the response regulator Rrp1, which produces c-di-GMP [13,19], at 23 °C [20], by glycerol [13,15], and in the tick [12]. RpoS and BadR both repress levels of *glp* operon transcripts, although BadR likely exerts its influence through RpoS [21,22]. Additionally, the c-di-GMP effector protein PlzA can either positively or negatively affect *glp* operon expression depending on its c-di-GMP-binding state [23]. These regulatory pathways targeting the *glp* operon represent the best understood strategies that *B. burgdorferi* uses to persist in the tick and illustrate the central role of glycerol regulation in this phase of the enzootic cycle. Other genes involved in carbohydrate utilization, such as *malQ* and *chbC*, are not required for *B. burgdorferi* in either its vertebrate host or tick vector [10,11].

GlpD shuttles G3P towards glycolysis via DHAP to provide energy while the reverse reaction, reducing DHAP to G3P mediated by another predicted G3PDH, GpsA, connects carbohydrates entering glycolysis to lipid and lipoprotein biosynthesis (Fig 1) [5–7]. In the absence of glycerol, GpsA, using carbohydrates from glycolysis, serves as the only known pathway to provide G3P for lipid and lipoprotein biosynthesis as *B. burgdorferi* cannot import this phosphorylated sugar alcohol or salvage glycerolipids [24]. *B. burgdorferi* must coordinate the activities of GlpD and GpsA to efficiently balance carbon sources and redox cofactors, such as NADH, and respond to the physiological requirements of the spirochete. Thus, the GlpD/GpsA metabolic node regulates carbon flow between lipid biosynthesis and glycolysis in response to the phase of the enzootic cycle as indicated by the available carbon sources.

In this study we examine the *in vivo* role of the GpsA/GlpD metabolic node in murine infectivity and tick persistence in an animal model of Lyme disease. Additionally, we molecularly dissect the contributions and interactions *in vitro* of these two G3PDHs in spirochete survival and morphology as well as broad metabolic regulation using a metabolomics approach.

Results

B. burgdorferi has a reduced genome resulting in limited metabolic capacity where the only identified connection of glycerol metabolism and lipid biosynthesis to glycolytic energy

production is the bidirectional oxidoreductase node mediated by the opposing actions of a pair of G3PDHs GlpD and GpsA (Fig 1) [5–7]. Based on sequence homology, GlpD is thought to oxidize G3P to DHAP and concomitantly reduce either NAD^+ or FAD. GpsA is predicted to catalyze the reverse reaction to reduce DHAP to G3P using the reducing power of NADH or NADPH. Pappas et al., 2011 [12] and He et al., 2011 [13] have shown that GlpD and the *glp* operon, respectively, are important for *B. burgdorferi* growth on glycerol and for persistence in the tick, but dispensable for murine infectivity. The function of GpsA either *in vitro* or *in vivo* has not previously been evaluated in *B. burgdorferi*.

***B. burgdorferi* *gpsA* complements the growth defect of an *Escherichia coli* *gpsA* mutant**

To genetically confirm the predicted function of *B. burgdorferi* GpsA, we heterologously complemented the growth phenotype of an *E. coli* *gpsA* mutant. The *B. burgdorferi* *gpsA* (*bb0368*) gene was cloned into the *E. coli* (Ec) isopropyl β -D-1-thiogalactopyranoside (ITPG)-inducible expression vector pUC18. The *E. coli* *gpsA* mutant BB20-14 [25], which is a G3P auxotroph and cannot grow on glucose as the sole carbon source, was made competent and transformed with either the empty vector, pUC18, or the vector carrying the *B. burgdorferi* *gpsA* gene, pUC18-*gpsA*_{Bb}. The strains Ec Δ *gpsA* (BB20-14), Ec Δ *gpsA*+pUC18 (empty vector) and Ec Δ *gpsA*+pUC18-*gpsA*_{Bb} (expressing *B. burgdorferi* *gpsA*) were inoculated at 5×10^7 cells ml^{-1} and grown in M9 minimal salts media (Fig 2A) or M9 minimal salts media with glucose (Fig 2B). Cultures were grown at 37°C for 9 h with the OD₆₀₀ taken every 17 min. In M9 media lacking a carbon source, all three strains grew at approximately the same rate and failed to grow exponentially or reach high cell density (Fig 2A). When glucose was added as the sole carbon source to the M9 media, only the strain expressing *B. burgdorferi* *gpsA* (Ec Δ *gpsA*+pUC18-*gpsA*_{Bb}) had sustained exponential growth and grew to high cell density ($>5 \times 10^8$ cells ml^{-1}) (Fig 2B). These data demonstrate that *B. burgdorferi* *gpsA* can heterologously complement the growth phenotype of an *E. coli* *gpsA* mutant on glucose as a sole carbon source, providing experimental support for the annotated function of *gpsA* in *B. burgdorferi*.

Δ *gpsA*, Δ *glpD* and Δ *gpsA*/ Δ *glpD* mutant strains have wild-type growth *in vitro*

To investigate the biological role of the metabolic node that interconverts G3P and DHAP regulated by GpsA and GlpD, the genes *gpsA* or *glpD* were mutated alone or together by allelic exchange with antibiotic resistance cassettes to generate Δ *gpsA*, Δ *glpD* and the double mutant Δ *gpsA*/ Δ *glpD* strains. All strains were complemented *in cis* to yield the full array of complemented strains: *gpsA* complemented (*gpsA*⁺), *glpD* complemented (*glpD*⁺), *gpsA* complemented in the Δ *gpsA*/ Δ *glpD* background (*gpsA*⁺/ Δ *glpD*), *glpD* complemented in the Δ *gpsA*/ Δ *glpD* background (Δ *gpsA*/*glpD*⁺) and both *gpsA* and *glpD* complemented in the Δ *gpsA*/ Δ *glpD* background (*gpsA*⁺/*glpD*⁺) (S1 Fig). Immunoblot analyses of the mutants using antibodies against GlpD and GpsA were used to confirm the deletion and complementation of the respective genes (S1H and S1I Fig). To genetically evaluate the role of *gpsA* and *glpD* during *in vitro* growth, cultures were grown in Barbour-Stoener-Kelly II media containing 6% rabbit serum (BSK + RS) for eight days and spirochetes were enumerated using a Petroff-Hauser cell counter. No statistical difference in growth was observed between wild-type, Δ *gpsA*, Δ *glpD* or the double mutant Δ *gpsA*/ Δ *glpD* strains after day one (Fig 3A). These data suggest that neither *gpsA* nor *glpD* play a significant role during *B. burgdorferi* growth in nutrient-rich media *in vitro*.

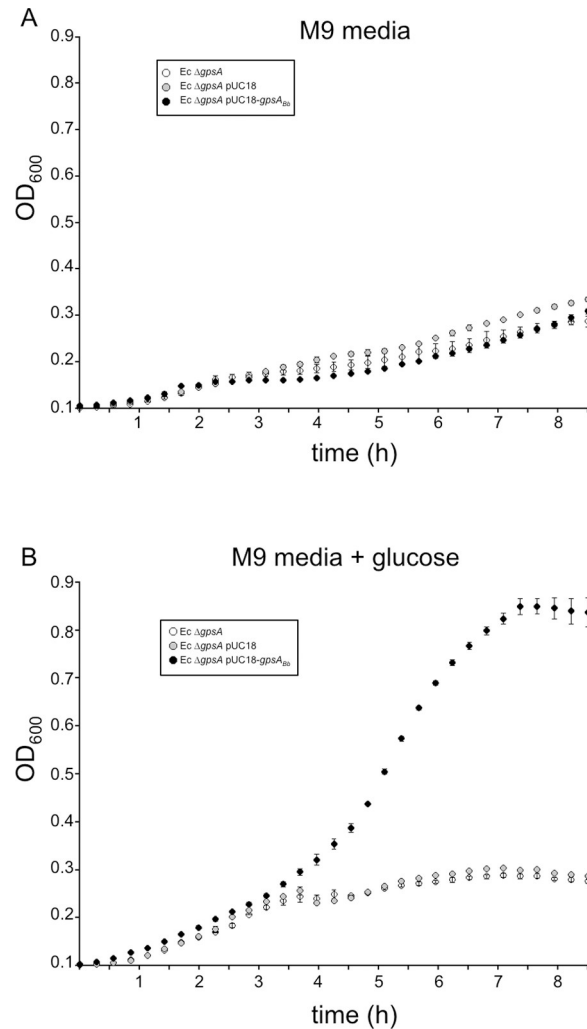


Fig 2. Heterologous complementation of an *E. coli* *gpsA* mutant with *B. burgdorferi* *gpsA* restores growth in glucose. The *E. coli* *gpsA* null mutant, strain BB20-14 (Ec Δ gpsA, white circles), *E. coli* *gpsA* null mutant with the inducible pUC18 expression vector (Ec Δ gpsA pUC18, gray circles) or *E. coli* *gpsA* null mutant with pUC18 carrying the *B. burgdorferi* *gpsA* gene (Ec Δ gpsA pUC18-*gpsA*_{Bb}) were grown in M9 minimal media containing 0.1 mM IPTG either without (A) or with 1% glucose (B) at 37°C. Cell density measurements (OD₆₀₀) were taken every 17 min. Data are the average from two separate cultures for each strain and error bars represent SEM; the experiment shown is representative of three independent biological replicates. The Ec Δ gpsA pUC18-*gpsA*_{Bb} strain had significantly higher ($p < 0.05$) OD₆₀₀ values compared to the other two strains from 4 h to 8 h of growth, as determined by one-way ANOVA with a Tukey's *post-hoc* test.

<https://doi.org/10.1371/journal.ppat.1010385.g002>

GpsA is required for survival during nutrient stress

We hypothesized that GpsA functions in survival during nutrient stress, an *in vitro* condition used to mimic the tick midgut environment between bloodmeals. To test this, *B. burgdorferi* strains were grown to $7\text{--}9 \times 10^7$ cells ml⁻¹ in normal growth medium, collected, resuspended and incubated in RPMI medium (which contains 2 mg ml⁻¹ glucose) for 24 h, as previously described [18]. Cells were plated in semi-solid BSK, and colonies allowed to grow for approximately two weeks before enumeration. *B. burgdorferi* survival is represented as the percentage survival after 24 h of nutrient stress compared to cells plated before nutrient stress (0 h). Δ gpsA mutants were almost completely compromised for survival during nutrient stress, while the

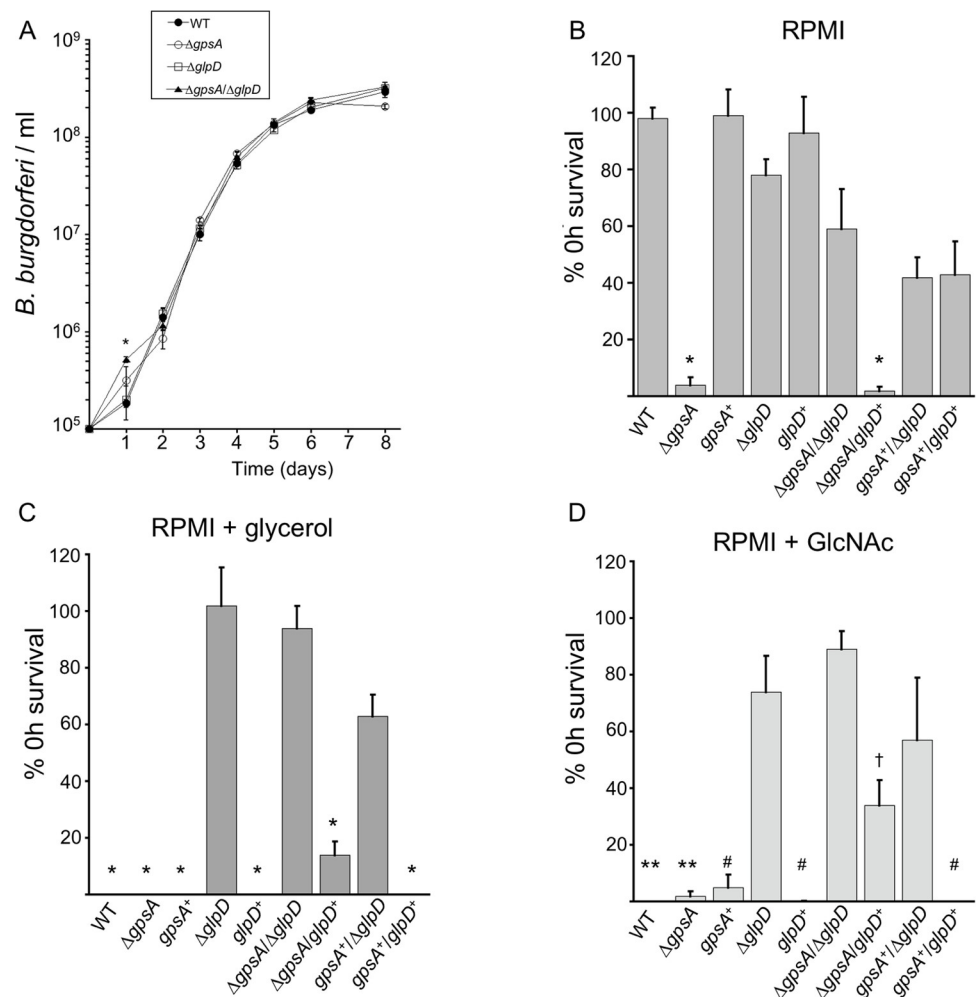


Fig 3. Growth of the *gpsA* and *glpD* mutants and survival under nutrient stress without or with different carbon sources *in vitro*. (A) *B. burgdorferi* strains were inoculated at 1×10^5 cells ml^{-1} in BSK + RS and grown at 35°C . Cells were enumerated every 24 h and cell density plotted over eight days. Data are the means from three independent biological replicates and error bars represent SEM. No significant difference in cell density was determined except at day 1 between the wild-type (WT) and Δ gpsA/ Δ glpD strains: * indicates $p = 0.046$ between the mean cell density of WT and Δ gpsA/ Δ glpD strains at day 1 as determined by one-way ANOVA with a Tukey's *post-hoc* test. Strains were grown in BSK + RS at 35°C (to a cell density of $5\text{--}9 \times 10^7$ cells ml^{-1}) before shifting to RPMI alone (B), or RPMI containing 0.4% glycerol (C) or 0.4% *N*-acetylglucosamine (GlcNAc) (D) and incubated at 35°C for 24 h. Cultures were plated in semi-solid BSK media and allowed to grow at 35°C in 5% CO_2 before colony enumeration. Data are presented as the percent survival of each strain before (0 h) shifting to the nutrient stress media. Data are the mean of at least three biological replicates and error bars represent the SEM. Significance determined by one-way ANOVA with a Tukey's *post-hoc* test. (* $p < 0.0001$; ** $p < 0.002$; # $p < 0.01$; † $p = 0.0075$).

<https://doi.org/10.1371/journal.ppat.1010385.g003>

Δ glpD mutant was not significantly affected compared to wild type (Fig 3B). This phenotype is restored in the *gpsA*⁺ and, surprisingly, in the Δ gpsA/ Δ glpD double mutant (Fig 3B). Complementing the double mutant with *glpD*, thus essentially constructing an independent *gpsA* mutant, also resulted in a *B. burgdorferi* strain unable to survive nutrient stress, similar to the Δ gpsA mutant (Δ gpsA/*glpD*⁺ Fig 3B). *gpsA* complementation of the double mutant and complete complementation of the double mutant significantly increased survival compared to Δ gpsA, but did not fully restore survival to wild-type levels (*gpsA*⁺/ Δ glpD and *gpsA*⁺/*glpD*⁺, Fig 3B). These data suggest that *gpsA* plays a crucial role in survival during nutrient stress in culture while *glpD* is dispensable. Furthermore, our results suggest we have identified the first

suppressor mutation in *B. burgdorferi* as deleting the *glpD* gene in a Δ *gpsA* mutant background restored viability under nutrient stress.

Because the link from glycolysis to G3P metabolism is severed in the Δ *gpsA* mutant, we determined if glycerol could restore survival of the *gpsA* mutant in nutrient stress medium (RPMI + glycerol). Strains were grown and treated as in Fig 3B except that 0.4% glycerol was added to the RPMI medium. Unexpectedly, glycerol in the nutrient stress medium was cytotoxic to wild-type *B. burgdorferi* (Fig 3C). In fact, glycerol was toxic to all strains except the Δ *glpD* mutants (Fig 3C), suggesting that metabolism of G3P by GlpD is necessary for the bactericidal activity of glycerol in this restrictive medium. Next, we examined if GlcNAc, a carbohydrate necessary for *in vitro* growth [9,10,26], could rescue the *gpsA* survival defect in RPMI medium. The results with GlcNAc were similar to those with glycerol: survival in GlcNAc was significantly compromised in almost all strains compared to those lacking *glpD* (Fig 3D). The *glpD* complement of the double Δ *gpsA*/ Δ *glpD* mutant (Δ *gpsA*/*glpD*⁺) was significantly compromised for survival compared to the Δ *gpsA*/ Δ *glpD* mutant (Fig 3D). GlcNAc is not predicted to be metabolized by the action of GlpD, suggesting an unidentified link between GlpD and the metabolism of GlcNAc, possibly involving redox cofactors involved in the GlpD/GpsA oxidoreductase node. Together these results illuminate the importance of the metabolic balance of the intermediates and cofactors involved in the GpsA/GlpD node in *B. burgdorferi* adaptation to and survival during changing carbohydrate availability.

The *gpsA* mutant displays increased round body formation and decreased reductase activity

To assess the redox potential of the G3PDH mutants, overall reductase activity in individual cells was monitored by microscopy using a fluorescent reporter. Wild-type and mutant strains were grown to $\sim 7\text{--}9 \times 10^7$ cells ml⁻¹, collected and incubated in RPMI medium (nutrient stress) for 16 h. Cultures were then incubated with BacLight RedoxSensor Green and propidium iodide for 10 min before wet-mounting live cells to be imaged by fluorescence microscopy. RedoxSensor Green stain fluoresces (shown as cyan in Fig 4) when reduced, indicating intracellular reductase activity and cell viability. Almost all (90%) wild-type cells in nutrient stress media for 16 h show reductase activity/viability while only about 30% of Δ *gpsA* cells fluoresce (cyan staining, Fig 4A, 4B, and 4F). Strikingly, Δ *gpsA* cells undergo a dramatic morphological change from flat-wave to a condensed spherical form called round bodies (RBs) during nutrient stress that is rarely seen in wild-type *B. burgdorferi* (Fig 4A, 4B, and 4F). The physiological role of RBs remains unknown but the transition is triggered by environmental stress and may be related to persistence, as this form has been observed *in vivo* in ticks [18,27–29]. Both the decrease in reductase activity and the increase in RB formation in Δ *gpsA* mutant cells are restored not only in the *gpsA*⁺ strain but also in the Δ *gpsA*/ Δ *glpD* double mutant (Figs 4C, 4D, and 4F), which is further evidence of *glpD* functioning as a suppressor mutation of the pleiotropic *gpsA* phenotypes. Deletion of the *glpD* gene alone affected neither reductase activity nor morphology during nutrient stress (Fig 4E and 4F). These data further support the findings that GpsA is important for cell survival under nutrient stress, a result likely reflected in reduced reductase activity. Additionally, the dramatic increase in RB formation of the Δ *gpsA* mutant is evidence that GpsA is a key modulator of morphological changes during nutrient stress.

A recent study has implicated GpsA in resistance of *Streptococcus pneumoniae* to oxidative stress [30]. To examine if *gpsA* also protects *B. burgdorferi* from oxidative stress, we measured the viability of wild-type, Δ *gpsA* and *gpsA*⁺ strains following exposure to H₂O₂ and found no significant differences between the strains, at least under the conditions tested (S2 Fig).

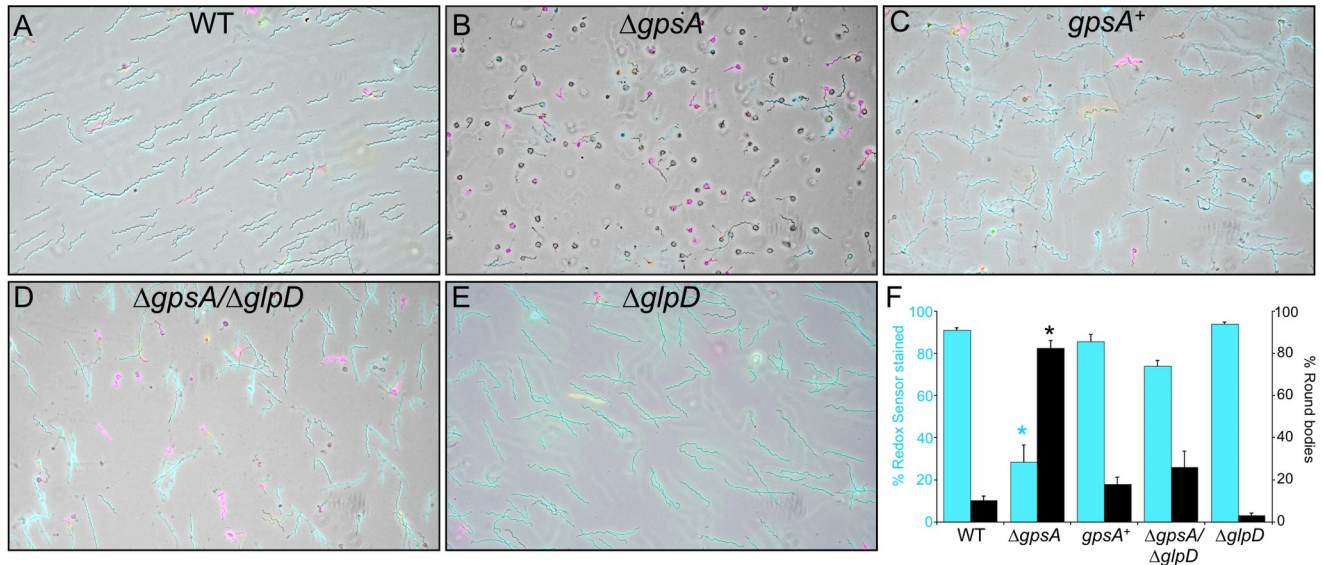


Fig 4. Decreased reductase activity and increased round body formation in the *gpsA* mutant. (A) Wild-type (WT), (B) $\Delta gpsA$ mutant, (C) $gpsA^+$ complement, (D) $\Delta gpsA/\Delta glpD$ double mutant and (E) $\Delta glpD$ mutant strains were grown in BSK + RS at 35°C (to a cell density of $5\text{--}9 \times 10^7$ cells ml^{-1}) before shifting to RPMI for 16 h at 35°C. Bacterial reductase activity was detected by staining with RedoxSensor Green and membrane integrity assessed by staining with propidium iodide (PI). Live cells were imaged by fluorescence microscopy for RedoxSensor Green (cyan) and PI (magenta) and overlaid with white light images. (F) The percentage of cells stained with RedoxSensor Green and the percentage of cells in round body (RB) form was quantified. Data are the mean of three biological replicates and error bars represent the SEM. Asterisks signify a significant difference ($p \leq 0.0001$) between the mean percent of RedoxSensor-stained $\Delta gpsA$ cells compared to all other strains and the mean percent of RBs in the $\Delta gpsA$ strain compared to all other strains as determined by one-way ANOVA with a Tukey's *post-hoc* test.

<https://doi.org/10.1371/journal.ppat.1010385.g004>

GpsA and GlpD influence the *B. burgdorferi* metabolome

To better understand how GpsA and GlpD affect the global physiology of *B. burgdorferi*, we performed semi-targeted metabolomics by liquid chromatography-tandem mass spectroscopy on the $\Delta gpsA$ and $\Delta glpD$ mutants in culture. Strains were grown in BSK + RS at 35°C to a density of $\sim 3 \times 10^7$ cells ml^{-1} before processing and analysis. Comparing the mutant metabolomes to wild type by unbiased principal component analysis, separate axes were readily observed that defined the metabolic effects of $\Delta gpsA$ versus the metabolic effects of $\Delta glpD$. Complements of both mutants resulted in a return toward wild type and the $\Delta gpsA/\Delta glpD$ double mutant comigrated with $\Delta glpD$ in agreement with the increased survival phenotype of the $\Delta gpsA/\Delta glpD$ double mutant (Fig 5A). The first principal component, which defines the separation of $\Delta gpsA$ from wild type, is heavily loaded by the opposing behavior of ATP and AMP, positively loaded for NADH, and negatively loaded with G3P and three-carbon glycolytic intermediates (Fig 5B). By contrast, $\Delta glpD$ separation along principal component two is positively loaded for G3P and negatively loaded for NADH in support of an opposing reaction directionality between GpsA and GlpD. Interestingly, both primary principal components are positively loaded for AMP and negatively loaded for ATP suggesting that proper functioning of the G3P arm of *B. burgdorferi* metabolism is essential for energy metabolism (Fig 5B).

In further support of the anticipated enzymatic function of GpsA, univariate analysis of the metabolite datasets showed that the largest metabolic changes in the $\Delta gpsA$ mutant compared to wild type were localized to the putative redox cofactor (NADH, 23.7-fold increase) and the anticipated product (G3P, 20.5-fold decrease) of GpsA (Fig 5C). Despite its predicted role as a substrate of GpsA, DHAP levels were only 1.7-fold higher in the $\Delta gpsA$ mutant. This smaller effect compared to G3P and NADH is likely due to triose phosphate isomerase converting

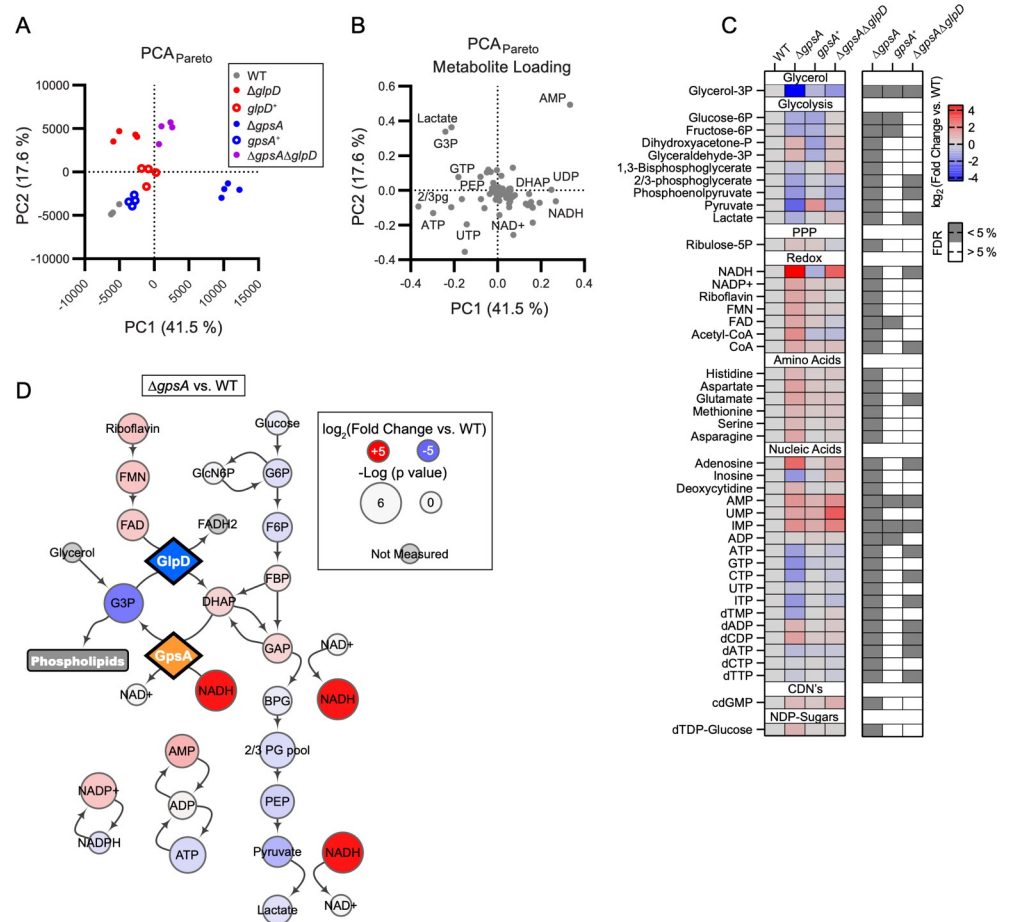


Fig 5. GpsA regulates central metabolism and redox balance. (A) Polar metabolomics of bacterial strains subjected to principal component (PC) analysis with pareto-scaling. (B) The corresponding metabolite loading distribution for the analysis displayed in (A) for principal components 1 and 2. (C) Metabolites that significantly vary between *ΔgpsA* and wild type (WT) with a false discovery rate (FDR) less than 5%. Values in the heatmap at left are displayed as the \log_2 (fold change mutant versus WT) and values in the accompanying heatmap at right indicate whether that metabolite passes a 5% FDR filter for the indicated comparison as assessed by a Benjamini-Hochberg correction. (D) Metabolic map of the changes in glycolysis and the glycerol shunt that occur with the loss of GpsA. All measured metabolites in the included pathways are displayed. The \log_2 (fold change *ΔgpsA* versus WT) is displayed as color of the node and the $-\log(p\text{-value})$ is displayed as the size of the node. Enzymes in the glycerol arm of metabolism are displayed as diamonds. Data are from four independent biological replicates.

<https://doi.org/10.1371/journal.ppat.1010385.g005>

DHAP to glyceraldehyde-3-phosphate (GAP) for glycolysis (Fig 5D). With the exceptions of DHAP, GAP, and fructose-1,6-bisphosphate, glycolytic intermediates, particularly pyruvate (6.6-fold decrease), were decreased in the *ΔgpsA* mutant. Concomitantly, ATP levels decreased (2.1-fold) and AMP levels increased (2.6-fold). These changes in glycolysis likely drive the decreased energy levels in the cell and may account for the susceptibility of the *ΔgpsA* mutant strain to nutrient stress (Fig 3). The complete list of metabolite levels in all the mutants is included (S2 Table).

The dramatic 23.7-fold increase in NADH levels in the *gpsA* mutant compared to wild type suggests that GpsA is a dominant regulator of NADH levels in *B. burgdorferi*. The dysregulation of glycolysis may be a consequence of these elevated levels of NADH, which would inhibit glyceraldehyde-3-phosphate dehydrogenase (GAPDH) and thus glycolysis in the *ΔgpsA* mutant [31] (Fig 5D). The changes in metabolite levels in the *ΔgpsA* mutant were largely

restored to wild-type levels in the *gpsA*⁺, but energy stress was still apparent in elevated AMP levels (Fig 5C). Metabolite levels in the Δ *gpsA*/ Δ *glpD* double mutant shifted toward wild-type levels, although not as completely as in the *gpsA*⁺. Univariate analysis further supported the action of GlpD as metabolically opposed to GpsA. While the metabolic phenotype in the Δ *glpD* mutant was of a smaller magnitude compared to the Δ *gpsA* mutant, DHAP levels in the Δ *glpD* mutant were 4.9-fold lower and G3P levels 4.2-fold higher than in the wild type (S3A Fig), supporting the predicted GlpD function. NADH levels were lower in the Δ *glpD* mutant, suggesting that either NADH is the reduced cofactor as G3P is oxidized to DHAP or that the effects of *glpD* deletion on GAP limit the recovery of NADH by GAPDH (S3B Fig). The effects on glycolysis in the Δ *glpD* mutant were localized to DHAP, GAP, phosphoenolpyruvate, and pyruvate (S3A Fig). Complementation of the Δ *glpD* mutant overcorrected the elevated levels of G3P and somewhat restored levels of NADH associated with *glpD* deletion suggesting the reintroduction of active enzyme (S3A Fig). However, dysregulation of glycolysis and energy metabolism was not restored between the Δ *glpD* mutant and the *glpD*⁺, indicating that there was only partial restoration of the wild-type phenotype even though *glpD* was complemented in *cis* with the native *glp* promoter.

GpsA regulates the NADH/NAD⁺ ratio

To confirm and quantify the GpsA-mediated regulation of nicotinamide cofactor levels observed in the metabolomics analysis, the NADH/NAD⁺ molar ratios in the Δ *gpsA* mutant were measured via an *in vitro* luminescence assay. Strains were grown and samples prepared as described for the metabolomics studies before measuring the NADH and NAD⁺ levels. The NADH/NAD⁺ molar ratio was approximately fourfold higher in the Δ *gpsA* mutant strain than in wild-type cells (Fig 6). This difference was fully restored in the *gpsA*⁺, but, curiously, not in the double Δ *gpsA*/ Δ *glpD* mutant strain (Fig 6). These data support the finding that *gpsA* highly regulates NADH levels in *B. burgdorferi* (Fig 5).

GpsA and GlpD levels are independent of each other

Because GpsA and GlpD catalyze the interconversion of G3P and DHAP, *B. burgdorferi* may respond to the mutation of one enzyme by altering the levels of the other G3PDH to compensate. To examine this possibility, levels of GpsA protein were examined in the Δ *glpD* mutant and levels of GlpD protein were examined in the Δ *gpsA* mutant by immunoblot analyses. Cell lysates analyzed from wild-type, Δ *glpD* mutant and *glpD*⁺ strains grown in normal growth medium (BSK + RS) at 35°C or incubated in nutrient stress medium (RPMI) showed no appreciable difference in GpsA protein levels (Fig 7A). FlaB was used as a loading control (Fig 7A and 7B). Similarly, GlpD levels did not change in the Δ *gpsA* mutant compared to the wild type or the *gpsA*⁺ under similar conditions (Fig 7B). Thus, GpsA and GlpD protein levels are independent of each other, at least during *in vitro* culture.

GpsA is required for murine infectivity

Because GpsA and GlpD dramatically affect *B. burgdorferi* metabolism, particularly NADH levels, we examined the role of this oxidoreductase cycle *in vivo* using the mouse-tick model of Lyme disease. To genetically assay the function of GpsA and GlpD in murine infection, 10⁴ cells of wild-type, Δ *gpsA*, *gpsA*⁺, Δ *glpD*, *glpD*⁺ and Δ *gpsA*/ Δ *glpD* strains were intradermally needle-inoculated in C3H-HeJ mice. Infection and dissemination were assessed via ear biopsies three weeks post-inoculation and tissues were cultured for *B. burgdorferi*. None of the mice injected with the Δ *gpsA* mutant were infected (Table 1).

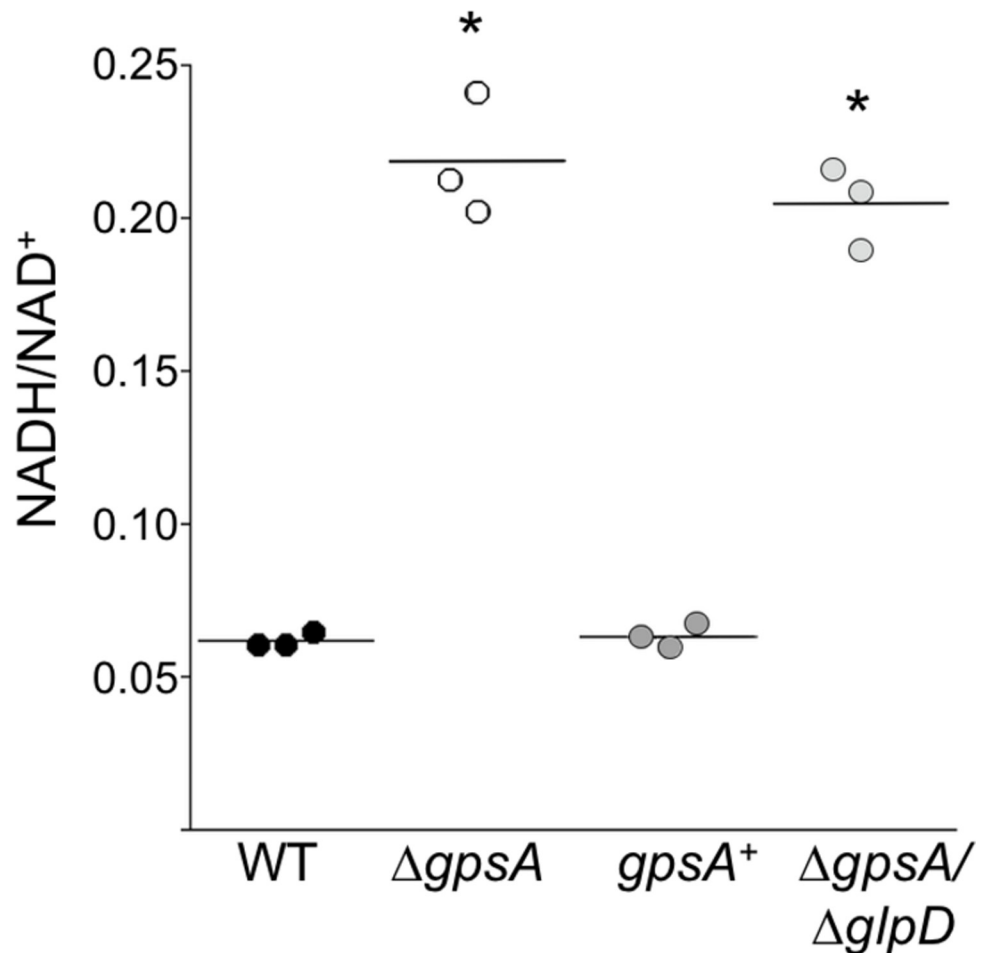


Fig 6. GpsA regulates NADH/NAD⁺ levels. Wild-type (WT, black circles), Δ *gpsA* mutant (Δ *gpsA*, white circles), *gpsA* complemented (*gpsA*⁺, dark gray circles) and Δ *gpsA*/ Δ *glpD* double mutant (light gray circles) strains were grown in BSK + RS at 35°C to $\sim 5 \times 10^7$ cells ml⁻¹ and NAD⁺ and NADH levels were measured with the NAD/NADH-Glo Assay. Each point represents a single biological replicate and bars represent the means. Asterisks represent a significant difference ($p < 0.0001$) in the means of NADH/NAD⁺ molar ratios of both the Δ *gpsA* mutant and the Δ *gpsA*/ Δ *glpD* double mutant compared to those of both the wild type and the *gpsA*⁺ determined by one-way ANOVA with a Tukey's *post-hoc* test.

<https://doi.org/10.1371/journal.ppat.1010385.g006>

Infectivity was restored in the *gpsA*⁺ but not in the Δ *gpsA*/ Δ *glpD* double mutant. Ear, ankle and bladder tissues were collected from the same mice five weeks post inoculation and cultured for *B. burgdorferi* to follow infectivity and dissemination. The results at five weeks were consistent with those at three weeks: the Δ *gpsA* mutant and Δ *gpsA*/ Δ *glpD* double mutant were still unable to establish infection (Table 1). Because GpsA is potentially involved in providing G3P for lipoprotein biosynthesis, we examined the levels of two lipoproteins, outer surface proteins A and C (OspA and OspC), in the Δ *gpsA* and Δ *gpsA*/ Δ *glpD* mutants. In strains grown *in vitro*, under the same conditions used for mouse infectivity studies, there was no appreciable difference in the levels of OspC or OspA (S4 Fig). The absence of *glpD* did not affect murine infectivity by needle inoculation, results agreeing with previous studies [12,13].

To determine if the infectivity defect of the Δ *gpsA* and Δ *gpsA*/ Δ *glpD* mutants could be overcome by increasing the challenge dose, mice were inoculated with 10^5 or 10^6 cells of each strain, and infectivity and dissemination monitored as described above at three and five weeks

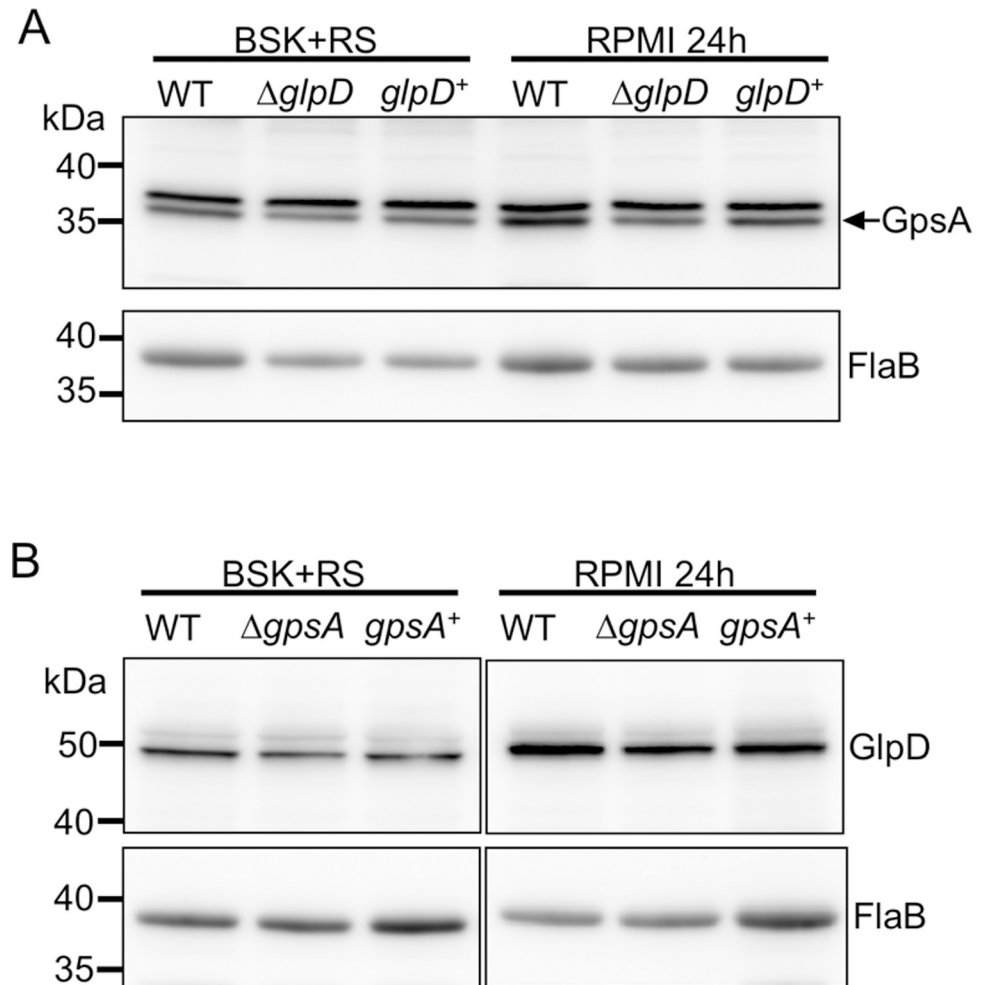


Fig 7. GpsA and GlpD levels are independent. (A) Wild-type (WT), $\Delta glpD$ mutant ($\Delta glpD$) and $glpD$ complemented ($glpD^+$) strains were grown in BSK + RS at 35°C or shifted to nutrient stress medium (RPMI) for 24 h before total cell lysates were collected. Samples were separated by SDS-PAGE and analyzed by immunoblot with antibodies against GpsA or FlaB (as a control). GpsA is the lower band of the doublet (see [S1H Fig](#)). (B) WT, $\Delta gpsA$ mutant ($\Delta gpsA$) and $gpsA$ complemented ($gpsA^+$) strains were grown and analyzed as in (A) except antibodies against GlpD were used for the immunoblots in the upper panels. Three independent experiments were done and representative data are shown.

<https://doi.org/10.1371/journal.ppat.1010385.g007>

after inoculation. The $\Delta gpsA$ mutant was noninfectious even with a dose of 10^6 cells ([Table 1](#)). At three weeks post challenge, *B. burgdorferi* could not be isolated from any mice injected with either 10^5 or 10^6 of $\Delta gpsA/\Delta glpD$ double mutants ([Table 1](#)). Surprisingly, five weeks after challenge with the higher doses of the $\Delta gpsA/\Delta glpD$ double mutant, 20/24 tissues were positive for *B. burgdorferi* re-isolation, indicating that deletion of $glpD$ suppresses the non-infectious phenotype of the $\Delta gpsA$ mutant, thus partially restoring infectivity, albeit with delayed kinetics. These data provide additional *in vivo* evidence that $glpD$ functions as a suppressor mutation of the non-infectious phenotype of the $\Delta gpsA$ mutant.

GpsA is crucial for persistence in the tick and transmission to mice

$gpsA$ is essential for survival during nutrient stress during *in vitro* cultivation ([Fig 3B, 3C, and 3D](#)); therefore, we hypothesized that $gpsA$ functions *in vivo* during persistence in the tick, when the spirochetes experience nutrient limitation after the tick absorbs the blood meal. To

Table 1. Infectivity by intradermal needle inoculation.

# cells injected	Strain	3 weeks		5 weeks	
		Ear	Ear	Ankle	Bladder
1×10^4	WT	3/4	3/4	3/4	3/4
1×10^4	$\Delta gpsA$	0/4	0/4	0/4	0/4
1×10^4	$gpsA^+$	4/4	4/4	4/4	4/4
1×10^4	$\Delta glpD$	4/4	4/4	4/4	4/4
1×10^4	$glpD^+$	3/4	3/4	3/4	3/4
1×10^4	$\Delta gpsA/\Delta glpD$	0/4	0/4	0/4	0/4
1×10^5	$\Delta gpsA$	0/4	0/4	0/4	0/4
1×10^6	$\Delta gpsA$	0/4	0/4	0/4	0/4
1×10^5	$\Delta gpsA/\Delta glpD$	0/4	3/4	4/4	3/4
1×10^6	$\Delta gpsA/\Delta glpD$	0/4	4/4	4/4	2/4

<https://doi.org/10.1371/journal.ppat.1010385.t001>

test this hypothesis, we artificially infected naïve larvae with wild-type, $\Delta gpsA$, $gpsA^+$ and $\Delta gpsA/\Delta glpD$ strains as previously described [32]. *B. burgdorferi* loads were measured in ticks through maturation and quantified by qPCR using primers to the *B. burgdorferi* *flaB* gene on DNA isolated from infected ticks. The $\Delta gpsA$ mutant was unable to establish a robust colonization in larvae compared to wild type and this deficiency was restored in the $gpsA^+$ (Fig 8A). The $\Delta gpsA/\Delta glpD$ double mutant was also compromised for colonization of larvae, indicating that this $\Delta gpsA$ mutant phenotype was not suppressed by the deletion of *glpD* (Fig 8A). Persistence through the molt from fed larvae to flat nymphs continued to be compromised in both the $\Delta gpsA$ mutant and the $\Delta gpsA/\Delta glpD$ double mutant compared to wild type and the $gpsA^+$, as *B. burgdorferi* loads fell to an average of less than 10 per tick (Fig 8B). Following feeding of infected nymphs on naïve mice, *B. burgdorferi* levels in $\Delta gpsA$ and $\Delta gpsA/\Delta glpD$ -infected ticks increased but remained greater than three orders of magnitude below those found in wild type and $gpsA^+$ -infected fed nymphs (Fig 8C). These *in vivo* data demonstrate a crucial, although not essential, role for *gpsA* to colonize and persist in ticks in the animal model of Lyme disease.

Transmission by tick bite is the natural route of *B. burgdorferi* infection of vertebrates. To examine the role of *gpsA* in transmission of *B. burgdorferi* from nymphs to naïve mice, three nymphs per mouse were allowed to feed until repletion. Murine infections were monitored three and five weeks post-feeding by culturing collected murine tissues as described above. The $\Delta gpsA$ mutant was not transmitted to mice (0/3 mice infected) and this defect was restored in the $gpsA^+$ strain (2/3 mice infected) (Table 2). The $\Delta gpsA/\Delta glpD$ double mutant was also compromised for transmission (0/3 mice infected) (Table 2), suggesting that *glpD* does not suppress the *gpsA* mutation in tick transmission.

Discussion

We have provided experimental evidence that the *B. burgdorferi* *gpsA* encodes a G3PDH, as predicted [5], by heterologously complementing an *E. coli* *gpsA* mutant (Fig 2). Our metabolomics analyses suggest that GpsA converts DHAP to G3P, as the $\Delta gpsA$ mutant showed reduced levels of G3P and increased levels of DHAP and NADH (Fig 5), providing additional evidence that *gpsA* encodes a G3PDH (or, based on the directionality of the reaction, a DHAP reductase). We also identified NADH as the likely cofactor of the redox reaction. Previous studies have shown that GlpD plays a role in growth on glycerol, but the substrates and products of GlpD have not been experimentally examined [12,13,15]. Here, our metabolomics analyses of the *glpD* mutant demonstrate a significant increase of G3P and decrease of DHAP levels compared to wild type, experimental evidence suggesting GlpD oxidizes G3P to DHAP. The lower

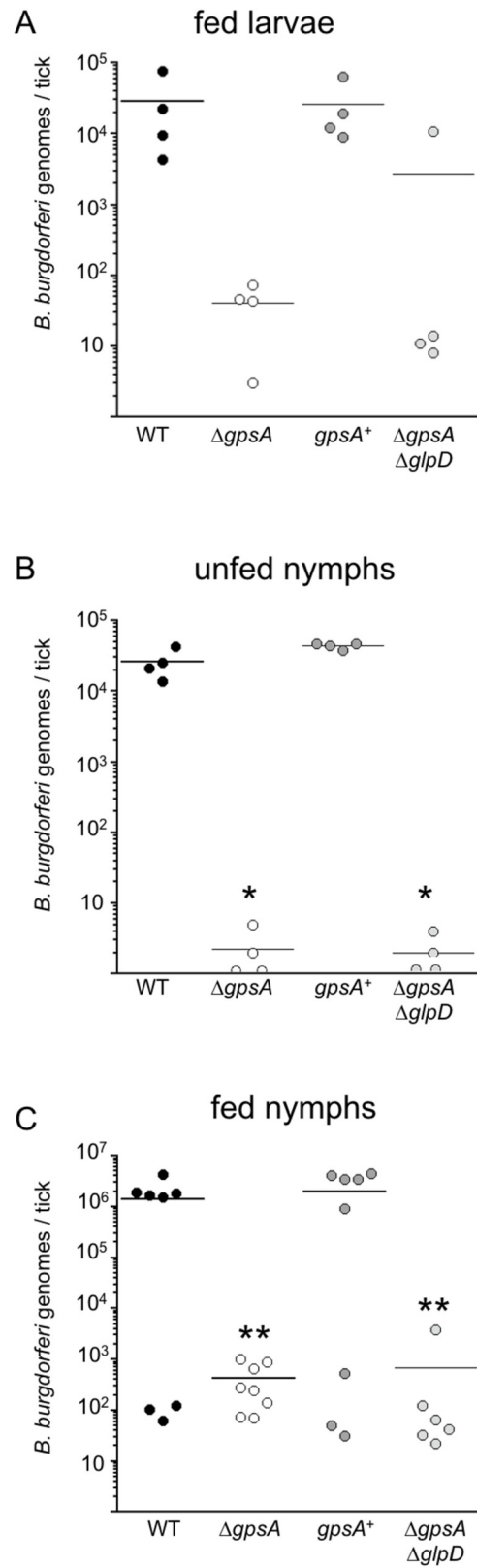


Fig 8. Persistence of the *gpsA* and *glpD* mutants in ticks. *B. burgdorferi* strains were introduced to larval ticks by immersion infection and fed on naïve mice. Acquisition and persistence of wild type (WT, black circles), Δ *gpsA* mutant (white circles), *gpsA* complement (*gpsA*⁺) (dark gray circles) and Δ *gpsA*/ Δ *glpD* double mutant (light gray circles) was assessed in ticks one week after larvae fed to repletion (A), following the molt to nymphs, nine weeks later (B) and one week after nymphs fed to repletion on naïve mice (C). DNA from infected ticks was isolated at each stage and *B. burgdorferi* load in ticks measured by TaqMan qPCR using primers/probe to *flaB*. Bars represent the mean of data points from a single experiment. The means of both the Δ *gpsA* and Δ *gpsA*/ Δ *glpD* mutants were significantly different (* $p < 0.0007$) from both the wild type and the *gpsA*⁺ determined by one-way ANOVA with a Tukey's *post-hoc* test in (B). The mean of the *gpsA*⁺ was significantly different (** $p \leq 0.03$) from both Δ *gpsA* and Δ *gpsA*/ Δ *glpD* mutants as determined by one-way ANOVA with a Tukey's *post-hoc* test in (C).

<https://doi.org/10.1371/journal.ppat.1010385.g008>

NADH levels seen in the Δ *glpD* strain suggest that NAD⁺ serves as the cofactor for oxidation of G3P by GlpD. An alternative possibility is that NAD⁺ is reduced downstream by a different cofactor, such as FADH₂, used by GlpD.

Metabolic virulence

The intersection of metabolism and virulence in microbial pathogens is gaining attention in the quest to define the molecular mechanisms responsible for causing disease [33]. In particular, bacterial glycerol metabolism and the associated physiological landscape can influence disease pathogenesis [34]. In the limited metabolic capacity of *B. burgdorferi*, glycerol metabolism plays an important role in the ability of the spirochete to traverse its enzootic cycle and, thus, the glycerol utilization genes are subject to complex regulation [5,7,8,16]. In this work we have presented evidence identifying a physiological linchpin connecting glycerol metabolism/lipid biosynthesis and glycolysis/energy generation that regulates stress survival *in vitro* and is crucial *in vivo* for both murine infectivity and persistence in the tick vector. This oxidoreductive node consists of two opposed G3PDHs, GpsA and GlpD, which catalyze the interconversion of G3P and DHAP, and likely communicates closely with the adjacent GAPDH. We found that *gpsA* is essential for disseminated infectivity in mice, by needle inoculation of up to 10⁶ cells (Table 1), and is crucial for persistence in ticks (Fig 8). Δ *gpsA* mutants and Δ *gpsA*/ Δ *glpD* double mutants were also compromised for transmission by nymphs, but the tick transmission phenotype is likely due, at least in part, to reduced spirochete loads in the tick. The infectivity phenotype may result from the inability of these mutant strains to establish infection at the inoculation (or tick bite) site or may reflect a defect in dissemination or persistence, but uncovering these details awaits further investigation. Additionally, a more detailed time course of Δ *gpsA* mutant and Δ *gpsA*/ Δ *glpD* double mutant replication during tick feeding may shed light on how these strains are unable to complete the vector-host lifecycle in the laboratory model of Lyme disease.

Recent studies have suggested that *gpsA* may be a virulence factor in other pathogens. Green et al., 2021 [30] found using a forward genetic screen that GpsA is important for *S. pneumoniae* to establish nasopharyngeal colonization and plays a role in resistance to oxidative stress. A G3PDH mutant strain of the plant pathogen *Acidovorax citrulli* showed reduced

Table 2. Infectivity by nymph bite.

strain	3 weeks		5 weeks	
	Ear	Ear	Ankle	Bladder
WT	3/3	3/3	3/3	3/3
Δ <i>gpsA</i>	0/3	0/3	0/3	0/3
<i>gpsA</i> ⁺	2/3	2/3	2/3	2/3
Δ <i>gpsA</i> / Δ <i>glpD</i>	0/3	0/3	0/3	0/3

<https://doi.org/10.1371/journal.ppat.1010385.t002>

virulence and increased resistance to antibiotics [35]. Additionally, a genome-wide mutagenesis screen identified a *gpsA* mutant in *Bartonella* that was avirulent, but the transposon insertion is upstream of the *gpsA* gene, complicating interpretations of the results [36]. Thus, GpsA activity, converting DHAP to G3P using a redox cofactor such as NADH, while not important for viability and growth under optimized culture conditions, represents a metabolic virulence factor important during the challenges of establishing host infection and resistance to immune defenses.

GlpD as a suppressor mutant

We have identified the *glpD* mutant as a suppressor of several *gpsA* mutant phenotypes, including murine infectivity by needle inoculation at high doses, restoration of viability under nutrient stress, and morphological changes. Much of the metabolic imbalance observed in our metabolomic studies of the Δ *gpsA* mutant were restored in the Δ *gpsA*/ Δ *glpD* double mutant, particularly the dramatic increase in NADH and decrease in G3P levels. Alleviating this imbalance by the absence of GlpD activity, which results in a decrease of NADH levels and an increase in G3P levels, may explain the suppression of the defects in the Δ *gpsA* mutant. There is precedent for the interdependence of *gpsA* and *glpD* in *E. coli*. The *gpsA* gene was thought to be essential in *E. coli* as mutants were not generated in a genome-wide, single gene deletion library known as the Keio collection [37]. However, deletion of the *gpsA* gene previously had been accomplished in a *glpD* mutant background in *E. coli* [38], supporting our assertion that *glpD* suppresses aspects of the pleiotropic *gpsA* mutant phenotype. Together, these findings suggest this node may be a common stress point, although bacteria with a more diverse metabolic repertoire may be better able to adjust for the metabolic imbalances created by genetic perturbation of either of these G3PDHs.

The *glpD* mutant suppressed some, but not all, of the defects of the *gpsA* mutant in the animal model of Lyme disease: infectivity by needle inoculation (10^5 and 10^6 cells) was restored, but persistence in ticks and transmission from nymphs to mice were not. These results suggest that certain requirements and/or signals in ticks cannot be overcome by complete disruption of the GpsA/GlpD node and likely require efficient carbon flow between glycolysis and lipid/lipoprotein biosynthesis. Even though levels of the outer membrane lipoproteins OspC and OspA were not affected *in vitro* in the Δ *gpsA* and Δ *gpsA*/ Δ *glpD* mutants, there may be differences in lipoprotein production *in vivo* that contribute to the defect in persistence in the tick.

The GpsA and GlpD metabolomes

Although the host metabolome in response to Lyme disease has been analyzed [39,40], here we report the first broad metabolomic datasets of *B. burgdorferi*, consisting of 129 metabolites. Our results identified GpsA as a dominant regulator of NADH levels and redox potential in the spirochete. The 23-fold increase in NADH in the Δ *gpsA* mutant compared to wild type was partially dependent on GlpD activity as levels were largely restored in the Δ *gpsA*/ Δ *glpD* double mutant (5.5-fold increase over wild type; Fig 5C). The redox state of the cell, reflected at least in part by the NADH/NAD⁺ ratio, is intimately entwined with glycolysis and secondary carbon metabolism [6,7]. Therefore, changes in the levels of glycolytic intermediates seen in the Δ *gpsA* mutant were likely a secondary effect of extremely high levels of NADH, a cofactor known to inhibit GAPDH activity [31]. This NADH-mediated inhibition could dramatically affect carbon flow in glycolysis. In fact, we found evidence to support this conclusion as levels of the two metabolites upstream of GAPDH, fructose-1,6-bisphosphate and GAP, were elevated and levels of all metabolites downstream were decreased. Again, in the Δ *gpsA*/ Δ *glpD* double mutant where levels of NADH were closer to those in wild-type cells, the levels of all

intermediates in glycolysis trended back toward wild-type levels, with the majority no longer significantly different. The same trend was observed in energy metabolism as represented by the levels of ATP, which could explain the differing viability *in vitro* under nutrient stress between the Δ *gpsA* mutant and the Δ *gpsA*/ Δ *glpD* double mutant (Fig 3B, 3C, and 3D).

The *B. burgdorferi* genome lacks the genes encoding the enzymes required for *de novo* NAD⁺ synthesis, but contains homologs of enzymes that convert nicotinamide to NAD⁺ (*pncA*, *pncB*, *nadD* and *nadE*), although a nicotinamide transporter has not yet been identified [5,6]. In the absence of an electron transport chain and reductive biosynthetic processes such as fatty acid synthesis, many routes of NADH oxidation are absent in *B. burgdorferi* [7]. The ability of *B. burgdorferi* to recycle NADH is further limited by the absence of genes encoding pyruvate dehydrogenase, lactate oxidase and pyruvate formate lyase. NAD⁺ can be recovered by lactate dehydrogenase converting pyruvate, formed in glycolysis, to lactate, which is then excreted from the cell through lactate permease [5]. The reverse reaction of converting lactate to pyruvate would regenerate NADH from NAD⁺. The constraints placed on the NAD⁺/NADH balance in *B. burgdorferi* likely result in increased sensitivity to disruption of this ratio and a greater need to recycle both the oxidized and reduced cofactors, particularly in glycolysis where NAD⁺ is used as an electron acceptor. GpsA represents one of the few enzymes identified in *B. burgdorferi* able to recycle NADH to NAD⁺, while at the same time supplying G3P, but at a cost to energy production from glycolysis.

NADH-dependent oxidative stress enzymes, such as coenzyme A disulfide reductase (CoADR) and superoxide dismutase (SodA) also can affect the redox state of the cell. CoADR is involved in reducing the disulfide form of coenzyme A occurring in an oxidative environment, using exclusively NADH [41]. The response of CoA-metabolites to *gpsA* deletion suggests that the glycerol oxidoreductase node and the CoADR systems are in metabolic communication, likely via NADH (Fig 5C). CoADR protects *B. burgdorferi* from lipid peroxidation, is essential for host infectivity and plays a role in survival in fed nymphs [41,42]. SodA in *B. burgdorferi* is required for murine infectivity, like *gpsA* and *cdr*, but the role in ticks has not been investigated [43]. A *sodA* deletion mutant has altered levels of NADH and NAD⁺, as well as ATP, but all were approximately twofold different from wild type [44]. Other NADH-dependent enzymes are present in *B. burgdorferi*, but many have not been studied or are presumed to be essential, and none have been shown to influence metabolite (NADH and G3P) levels to the degree observed in the Δ *gpsA* mutant.

Increased round body formation

B. burgdorferi morphology can change from the signature flat wave to RBs *in vitro* in response to environmental conditions, including nutrient stress [18,27,28,45] and *in vivo* in the tick [29] to presumably aid in *B. burgdorferi* persistence. RBs are a condensed spherical form of *B. burgdorferi* within an outer membrane that are viable and transitory [18,27–29]. The stringent response intracellular second messenger (p)ppGpp and the alternative sigma factor RpoS have been shown to control RB formation, as disrupting these global transcriptional regulators increased RB formation [18,29]. Cellular physiology also appears to be important as mutation of CoADR increases RB formation [42] and levels of acetyl-CoA and CoA are elevated in the Δ *gpsA* mutant (Fig 5C). Our results showing a massive transition of the Δ *gpsA* mutant to RBs during nutrient stress identify another metabolic enzyme involved in this morphologic change. Disruption of the redox potential of the cell may be a crucial signal for RB formation as both GpsA and CoADR use NADH as a cofactor and NADH levels dramatically increase and viability/reductase activity decrease in the Δ *gpsA* mutant (Fig 4, 5, and 6). Notably, many of the genes that regulate RB formation, *relB_{bu}*, *cdr* and *gpsA*, are also important for persistence in the

tick. The RB is not simply an aberrant non-viable form as many RBs remain viable (Fig 4) and can revert back to flat wave morphological forms [18,29,45]. Thus, environmental stresses that significantly alter the redox potential of the cell could trigger RB formation to aid survival under harsh conditions, such as in the tick between blood meals, but the mechanism and benefits of this morphological transformation for *B. burgdorferi* remain to be determined.

Compromised survival *in vitro* and *in vivo* during persistence in ticks

B. burgdorferi must adapt to the stress of depleted nutrients in the tick midgut as the blood meal is consumed following larval and nymphal feeding. We and others have used RPMI *in vitro* to mimic the nutrient stress experienced in the tick midgut between blood meals and have identified the Rel_{Bbu}-mediated stringent response and its effector DksA as important for survival under these conditions [17,18]. Here we found that *gpsA*, while not necessary for growth in nutrient-rich medium, was crucial for survival during nutrient stress *in vitro*, suggesting that NADH levels and redox potential have a key role in adapting to nutrient limitation. Completely severing the G3PDH node in the Δ *gpsA*/ Δ *glpD* double mutant partially restored NADH levels and rescued both the survival defect and reductase activity, indicating that the inability to shuttle DHAP to G3P for lipid biosynthesis was not the cause of cell death *in vitro*. Also, the metabolome of the Δ *glpD* mutant showed altered levels of both G3P and DHAP (S3 Fig) but this mutant was neither compromised for survival nor reductase activity, suggesting the changes in these metabolites were not involved in adapting to nutrient stress. Furthermore, the increased levels of NADH in the Δ *gpsA* mutant could have theoretically increased the resistance to peroxide, but that was not observed under our conditions (S2 Fig). Other redox enzymes using NAD⁺/NADH as a cofactor play a role in *B. burgdorferi* survival in response to environmental stresses, particularly oxidative stress. The CoADR mutant had a growth defect *in vitro* and was more susceptible to lipid peroxidation, but not reactive oxygen species, and a *sodA* mutant was also more susceptible to superoxide radicals [41–43,46]. Thus, oxidoreductase enzymes using NAD⁺/NADH as a cofactor likely play a variety of roles in adapting to external stresses encountered throughout the enzootic environment.

Because decreased levels of G3P, needed for lipid and lipoprotein biosynthesis, in the Δ *gpsA* mutant could account for the survival defect observed under nutrient stress, we added glycerol to RPMI in an attempt to chemically rescue the phenotype. Surprisingly, even in wild-type *B. burgdorferi*, glycerol was cytotoxic in nutrient stress media (Fig 3C). Furthermore, glycerol was cytotoxic to all strains except those lacking *glpD* (Δ *glpD*, Δ *gpsA*/ Δ *glpD* and *gpsA*⁺/ Δ *glpD*; Fig 3C), indicating that GlpD was necessary for glycerol-mediated cell death. The cytotoxicity of glycerol may be due the continued action of GlpD oxidizing G3P to feed glycolysis, which amplifies the deficit of NAD⁺. Even more unexpected was the finding that added GlcNAc produced the same *glpD*-dependent cell death phenotype (Fig 3D). Because there is no known shared metabolic pathway between transport or metabolism of GlcNAc and transport or metabolism of glycerol (until glycolysis), we hypothesize that cofactor dysregulation in nutrient-depleted media may cause cell death. Perhaps the addition of another nutrient to the media could rescue *B. burgdorferi* viability by restoring the metabolic balance, but these studies remain to be done.

gpsA is also crucial for persistence *in vivo* in the tick: *gpsA* mutants seem to have difficulty colonizing larvae, although the difference from wild type-infected larvae was not significant, and the mutants were severely compromised (1000–10,000-fold) for persistence in unfed nymphs and replication in fed nymphs (Fig 8). Again, the dysregulation of the redox potential and NADH levels may explain the persistence defect as similar pathways have been identified as important in other studies. CoADR and Dps/NapA/BicA involved in the oxidative stress

response were both shown to function during persistence in feeding nymphs [42,47]. Glycerol metabolism has been shown to be important for persistence in ticks [12,13], as *glpD* mutants have a threefold survival defect in fed larvae [14] and ten- to fifteenfold survival defect following nymph feeding [13]. The degree of dysregulation of NADH/NAD⁺ levels correlates with the severity of the persistence defect, suggesting this could be driving the tick phenotype. Unlike our *in vitro* results, the persistence defect in ticks was not restored in the Δ *gpsA*/ Δ *glpD* double mutant indicating that there are additional challenges in the tick environment that the double mutant is unable to overcome. The defect in persistence in the tick could also be explained by compromised lipid and lipoprotein production in the *gpsA* mutant strains. The biosynthetic lipid and lipoprotein pathways, including GlpF, GlpK, 1-acyl-G3P acyltransferase (*bb0037*), and two fatty acid CoA ligases (*bb0137* and *bb0593*), are induced in ticks compared to mammalian hosts, suggesting an important role in the vector [48]. Thus, disruption of G3P production in the *gpsA* mutants may stress the lipid/lipoprotein biosynthetic machinery resulting in decreased viability and persistence. Taken together, our studies and previous work highlight the importance of this metabolic node for persistence in the tick vector and infectivity in the vertebrate host.

Materials and methods

Ethics statement

All animal experiments were approved by the University of Montana Institutional Animal Care and Use committee and followed the *Guidelines for the Care and Use of Laboratory Animals* from the National Institutes of Health.

B. burgdorferi strains and growth conditions

Low-passage *B. burgdorferi* B31-5A4 [49], and genetically manipulated derivatives were grown and maintained in Barbour-Stoenner-Kelly II (BSK) liquid medium, pH 7.6, containing 6% rabbit serum (RS) (Pel-Freez Biologicals) [26] without gelatin. Cultures were grown at 35°C to $5\text{--}9 \times 10^7$ cells ml⁻¹ for experiments. Cells were enumerated using a Petroff-Hausser cell counting chamber [50].

B. burgdorferi strain construction

The parental strain B31-5A4, referred to as wild type, was used to construct all mutant strains. *E. coli* TOP10F' grown in lysogeny broth [51] were used for cloning. To construct the *gpsA* null mutant strain the regions upstream and downstream of the *gpsA* gene were amplified by PCR using KOD polymerase (Novagen) and the primers *gpsA*_U886F/*gpsA*_41R+AatII+AgeI or *gpsA*_1051F+AatII/*gpsA*_D1924R+AgeI (S1 Table), respectively, and B31-5A4 genomic DNA as a template. PCR products were cloned into pCR2.1-TOPO (Invitrogen) and verified by DNA-sequencing. Using the artificially engineered AgeI and AatII restriction sites, the two cloned PCR products were digested with AatII and AgeI and ligated together at the junction of the AatII site. The streptomycin/spectinomycin resistant cassette with the *flgB* promoter from *B. burgdorferi* [52] and *trpL* terminator from *Bacillus subtilis* [53] (*flgBp-aadA-trpLt*) containing flanking AatII sites was placed between the upstream and downstream DNA segments. The plasmid containing the *aadA* cassette replacing *gpsA* was purified and linearized using the restriction enzyme AhdI before electroporating competent B31-5A4 cells. 24 h after transformation, cells were plated in liquid BSK + RS in 96-well plates and transformants selected with 50 μ g ml⁻¹ streptomycin [54]. Colonies resistant to streptomycin were screened for the absence of *gpsA* by PCR analysis using the primers *gpsA*_U87F and *gpsA*_D1174R (S1B Fig). To

generate the *gpsA* *cis*-complemented strain, the entire *gpsA* ORF and promoter were amplified by PCR using the primers *gpsA*_U886F and *gpsA*_D1125R+AatII+AgeI to yield the upstream segment. PCR amplification using the primers *gpsA*_1051F+AatII and *gpsA*_D1924+AgeI were used to produce the downstream fragment. As described above, these segments were ligated together and a gene conferring resistance to kanamycin (*flgBp-aphI-trpLt*) inserted downstream of the *gpsA* gene. The resulting plasmid was purified, linearized, and electroporated into competent Δ *gpsA* mutant cells, which were plated as described above except that transformants were selected in 200 $\mu\text{g ml}^{-1}$ kanamycin. Restoration of the *gpsA* gene in isolated clones was confirmed by PCR analyses using the primers *gpsA*_U87F and *gpsA*_D1174R (S1B Fig).

The *glpD* null mutant strain was constructed as described above for the *gpsA* null mutant except that the primers *glpD*_U1016F and *glpD*_10R+AatII+AgeI were used to make the upstream segment and *glpD*_1568F+AatII and *glpD*_D2523R+AgeI were used to make the downstream segment. The gene conferring gentamicin resistance (*flgBp-aacC1-trpLt*) was inserted and transformants selected in 50 $\mu\text{g ml}^{-1}$ gentamicin. Clones resistant to gentamicin were screened by PCR for the absence of the *glpD* gene using the primers *glpD*_U56F and *glpD*_D1669R (S1D Fig). The *glpD* *cis*-complemented strain was constructed as described for the *gpsA* complement except the upstream and downstream segments were amplified by PCR using the primers *glpD*_U719F/*glpD*_D1613R+AatII+AgeI and *glpD*_D1611F+AatII and *glpD*_D2523R+AgeI, respectively (S1 Table). The *flgBp-aphI-trpLt I* gene was inserted downstream of the *glpD* gene and transformants selected in kanamycin and clones screened by PCR using the primers *glpD*_U56F and *glpD*_D1669R (S1C and S1D Fig and S1 Table). Competent Δ *gpsA* mutant cells were transformed with the construct described above and selected in gentamicin to generate the Δ *gpsA*/ Δ *glpD* double mutant strain. The same strategy used to make the *gpsA* complemented strain was used to make the *gpsA* complement of the double Δ *gpsA*/ Δ *glpD* mutant to yield the *gpsA*⁺/ Δ *glpD* strain. Likewise, the *glpD* complement of the double Δ *gpsA*/ Δ *glpD* mutant to generate the Δ *gpsA*/*glpD*⁺ strain was as described above. The *gpsA* and *glpD* double complement of the Δ *gpsA*/ Δ *glpD* double mutant was made by transforming competent *gpsA*⁺/ Δ *glpD* cells described above with a *glpD* complement construct described above except that a streptomycin resistance cassette (*flgBp-aadA-trpLt*) was used and transformants selected in streptomycin. Absence of the *gpsA* gene in the double Δ *gpsA*/ Δ *glpD* strain and restoration of the *gpsA* gene in the *gpsA*⁺/ Δ *glpD* and double complemented *gpsA*⁺/*glpD*⁺ isolated clones was confirmed by PCR analyses using the primers *gpsA*_385F and *gpsA*_493R (S1F Fig). Absence of the *glpD* gene in the Δ *gpsA*/ Δ *glpD* double mutant and restoration of the *glpD* gene in the Δ *gpsA*/*glpD*⁺ single complement and *gpsA*⁺/*glpD*⁺ double complement was confirmed by PCR using the primers *glpD*_1F+SacI and *glpD*_1267R+AatII (S1G Fig). All strains used for infectivity experiments were screened for the presence of plasmids important for murine infectivity and persistence in the tick [55].

Heterologous expression of *B. burgdorferi* *gpsA* in *E. coli* and growth analyses

The *B. burgdorferi* *gpsA* gene was amplified by PCR using KOD polymerase and the primers *gpsA*_1F+SacI and *gpsA*_1092R+PstI (S1 Table). The PCR product was cloned into pCR2.1-TOPO (Invitrogen) and verified by DNA sequencing. The *gpsA* gene was inserted into the multiple cloning site of the expression vector pUC18 by digesting both with the restriction enzymes PstI and SacI followed by ligation. The resulting pUC18-*gpsA*_{Bb} or the empty vector pUC18 were transformed into a *gpsA* null mutant *E. coli* strain (CGSC # 5424, *E. coli* Genetic Stock Center, Yale University) [25]. The *E. coli* strains Δ *gpsA*, Δ *gpsA* + pUC18 and Δ *gpsA*

+ pUC18-*gpsA*_{Bb} were grown in M9 minimal salts media containing 1% casamino acids with or without 1% glucose. To induce *gpsA*_{Bb} expression, 0.1 mM IPTG was added to all cultures. Cultures were grown in 96-well plates at 37°C with constant shaking in a BioTek Synergy HT plate reader (Agilent) where the OD₆₀₀ was measured every 17 min.

Nutrient stress and semi-solid BSK plating assay

B. burgdorferi strains were grown to $4-9 \times 10^7$ cells ml⁻¹, a portion diluted in BSK (approximately 200 spirochetes), and plated in semi-solid BSK (0 h time point). The remaining cultures were collected by centrifugation at 8000 x g for 10 min at 4°C. Cells were resuspended in RPMI 1640 without L-glutamine (Corning) either without or with 0.4% glycerol (Fisher Scientific) or 0.4% *N*-acetylglucosamine (MP Biomedicals) for nutrient stress assays as previously described [18]. After 24 h at 35°C cells, were diluted in BSK and plated in semi-solid BSK (24 h time points) and all plates (0 h and 24 h) allowed to grow at 35°C for about 14 days in a 5% CO₂ incubator before colony enumeration.

RedoxSensor staining and microscopy

B. burgdorferi strains were grown in BSK + RS at 35°C to $\sim 7 \times 10^7$ cells ml⁻¹ before collection at 8,000 x g for 10 min at 4°C. Cell pellets were resuspended in warm RPMI and incubated at 35°C for 16 h. Cultures were then stained with BacLight RedoxSensor Green and propidium iodide according to the manufacturer's instructions (1 μl RedoxSensor Green and 1 μl propidium iodide in 1.0 ml culture) from the BacLight RedoxSensor Green Vitality kit (Invitrogen). Cells were stained for 10 min at 35°C, collected by centrifugation (13,000 x g, 5 min, 4°C) and cell pellets resuspended in 1.0 ml PBS. 10 μl of cells were wet-mounted on a slide and live cells imaged using an Olympus BX51 fluorescence microscope with 100x/1.30 NA objective. Images were processed using ImageJ (National Institutes of Health; <http://rsbweb.nih.gov/ij/>) and Pixelmator (Pixelmator Team, Ltd). The mean percent cells stained with RedoxSensor Green and mean percent round body (RB) cells were determined from three independent biological replicates where at least 100 cells were enumerated for each strain. Significant difference between the means was determined by one-way ANOVA with a Tukey's *post-hoc* test.

Metabolomic analyses

For all liquid chromatography-mass spectrometry (LCMS) methods, LCMS grade solvents were used. Tributylamine and all synthetic molecular references were purchased from Millipore Sigma. LCMS grade water, methanol, isopropanol and acetic acid were purchased through Fisher Scientific.

B. burgdorferi strains were grown in BSK + RS at 35°C to $\sim 3 \times 10^7$ cells ml⁻¹ before collection at 8,000 x g for 10 min at 4°C. Cells were washed twice with HEPES-NaCl buffer and pellets were flash frozen in dry-ice and ethanol and stored at -80°C until processing. To process cells for metabolomic analysis, cell pellets were thawed on ice, resuspended in 150 μL ice-cold methanol (Sigma) and then incubated at room temperature for 10 min. Following incubation an equal volume of LCMS grade water was added and the samples were vigorously vortexed, then centrifuged at 13,000 x g for 15 min. Supernatants were collected, filtered in a 0.2 μM nitrocellulose syringe filter (GE Healthcare), and then diluted 1:3 before analysis. All samples were separated using a SCIEX ExionLC AC system and measured using a SCIEX 5500 QTRAP mass spectrometer. Polar metabolites were analyzed using a previously established ion pairing method with modification [56,57]. Quality control samples were injected after every 10 injections to control for signal stability. Samples were separated with a Waters Atlantis T3 column (100Å, 3 μm, 3 mm X 100 mm) using a binary gradient from 5 mM tributylamine, 5 mM acetic

acid in 2% isopropanol, 5% methanol, 93% water (v/v) to 100% isopropanol over 15 minutes. Each metabolite was identified and measured with two ion fragmentation pairs and a defined retention time.

All signals were integrated using MultiQuant Software 3.0.3. Signals with greater than 50% missing values were discarded and remaining missing values were replaced with the lowest registered signal value. All signals with a QC coefficient of variance greater than 30% were discarded. Metabolites with multiple ion pairs were quantified with the signature that displayed the highest signal to noise. All filtered datasets normalized against the total signal sum for the injection prior to analysis. Single and multi-variate analyses were performed in MarkerView Software 1.3.1. All univariate comparisons were subjected to a Benjamini-Hochberg cut-off at a false discovery rate of 5%.

NAD⁺/NADH assays

B. burgdorferi strains were grown at 35°C to $\sim 5 \times 10^7$ cells ml⁻¹ before collection at 14,000 x g for 10 min at 4°C. Cell pellets were washed twice with 1.0 ml cold H-N buffer (50 mM HEPES, 50 mM NaCl, pH 7.6), 15,800 x g, 5 min at 4°C, in cryovials. The supernatant was discarded and cell pellet flash frozen in liquid N₂ and stored at -80°C. Samples were solubilized and NAD⁺ and NADH levels measured separately using the NAD/NADH-Glo Assay Kit (Promega) according to the manufacturer's instructions. Luminescence was measured using a BMG Labtech/CLARIOstar plate reader. The levels of NAD⁺ and NADH were normalized to cell number from three independent biological replicates. Significant difference between the means was determined by one-way ANOVA with a Tukey's *post-hoc* test.

Immunoblot analyses

Equivalent amounts of *B. burgdorferi* whole cell extracts were analyzed by SDS-PAGE using Novex 4–20% Tris-Glycine polyacrylamide gels (Invitrogen) and proteins transferred to PVDF Immobilon membranes (Millipore). Membranes were blocked overnight at 4°C in blocking buffer (also used to dilute antibodies), which consisted of dPBS + 0.5% Tween-20 + 4% dried milk + 1% goat serum. Membranes were probed with rabbit anti-OspC (1:1000), mouse anti-OspA antibodies (1,2500, CDC), mouse anti-FlaB (1,100, gift from Tom Schwan), rabbit anti-GpsA (1:1000) or rabbit anti-GlpD (1,1000) followed by goat anti-rabbit or goat anti-mouse HRP-linked antibodies (Bio-Rad Laboratories) (1,10,000). Anti-GpsA and anti-GlpD antibodies were produced by GenScript using *B. hermsii* peptides as antigens. Detection was done by chemiluminescence (Amersham ECL Prime, GE Healthcare) and visualized using an LAS-3000 Intelligent Dark Box (Fujifilm Medical Systems USA).

Mouse infectivity by needle inoculation and tick transmission

C3H-HeJ mice (Charles River Laboratories) were intradermal injected with 1×10^4 to 1×10^6 *B. burgdorferi* cells grown at 35°C to cell densities of $5\text{--}9 \times 10^7$ cells ml⁻¹. Infection was determined by culturing mouse ear biopsies in BSK II containing 50 µg ml⁻¹ rifampicin, 20 µg ml⁻¹ phosphomycin and 2.5 µg ml⁻¹ amphotericin B and examining cultures by dark-field microscopy for the presence of spirochetes for 14 days. Five weeks post-infection, mice were sacrificed and ear, ankle and bladder tissues were collected, cultured and examined for spirochetes. Uninfected *Ixodes scapularis* larvae (National Tick Research and Education Resource, Oklahoma State University) were maintained in a 98% humidified chamber. To allow ticks to acquire *B. burgdorferi*, approximately 100 larvae per mouse were allowed to feed to repletion. Spirochete loads per tick were quantified by qPCR as described below. After infected larvae molted into nymphs (about 8 weeks), three mice were infested with three nymphs each and

allowed to feed to repletion. Murine transmission was monitored by culturing ear, ankle and bladder tissues as described above. Persistence of *B. burgdorferi* in ticks was followed by qPCR as described below.

Quantification of *B. burgdorferi* in ticks

Spirochete burdens in artificially infected ticks were assessed in fed larvae (one week, in groups of five), unfed nymphs (in groups of five) and fed nymphs (one week post feeding to repletion). DNA was extracted from ticks using the DNeasy Blood/Tissue kit (Qiagen) and the number of *B. burgdorferi* genomes in each tick determined by TaqMan qPCR with primers flaB_425F and flaB_542R and the flaB probe to the *flaB* gene (S1 Table) were 1 copy of *flaB* = one genome as previously described [18].

Supporting information

S1 Table. Oligonucleotides and probes used in this study.

(DOCX)

S2 Table. Metabolomic Analyses.

(XLSX)

S1 Fig. Strain construction and analyses. (A) Illustration of the *gpsA* mutant (Δ *gpsA*) and *gpsA* complemented (*gpsA*⁺) strains constructed by homologous recombination. The *gpsA* gene (*bb0368*) was replaced with the *B. burgdorferi* promoter from *flgB* fused to *aadA*, a gene conferring resistance to streptomycin (strep^R). A wild-type copy of *gpsA* was reintroduced in *cis* using the *B. burgdorferi* promoter from *flgB* fused to *aphI*, a gene conferring resistance to kanamycin (kan^R) to yield the *gpsA*⁺ strain. (B) Genomic DNA isolated from wild-type (WT), Δ *gpsA* and *gpsA*⁺ strains, and a no template control (NTC) was analyzed by PCR using primers 1 (*gpsA*_U87F) and 2 (*gpsA*_D1174R). (C) Illustration of the *glpD* mutant (Δ *glpD*) and *glpD* complemented (*glpD*⁺) strains constructed by homologous recombination. The *glpD* gene (*bb0243*) was replaced with the *B. burgdorferi* promoter from *flgB* fused to *aacC1*, a gene conferring resistance to gentamicin (gent^R). A wild-type copy of *glpD* was reintroduced in *cis* using the *B. burgdorferi* promoter from *flgB* fused to *aadA*, a gene conferring resistance to streptomycin (strep^R) to yield the *glpD*⁺ strain. (D) Genomic DNA isolated from WT, Δ *glpD* and *glpD*⁺ strains, and a NTC was analyzed by PCR using primers 3 (*glpD*_U56F) and 4 (*glpD*_D1669R). (E) Illustration of the double *gpsA*/*glpD* mutant (Δ *gpsA*/ Δ *glpD*) and single and double complemented strains constructed by homologous recombination as described above. The *gpsA* complement of the double mutant (*gpsA*⁺/ Δ *glpD*) was used to construct the *gpsA*-*glpD* double complement (*gpsA*⁺/*glpD*⁺). (F) Genomic DNA isolated from WT, the double *gpsA*/*glpD* mutant (Δ *gpsA*/ Δ *glpD*), the *gpsA* complement of the double mutant (*gpsA*⁺/ Δ *glpD*) and the *gpsA* and *glpD* double complement of the double mutant (*gpsA*⁺/*glpD*⁺) strains, and a NTC was analyzed by PCR using primers 5 (*gpsA*_385F) and 6 (*gpsA*_493R). (G) Genomic DNA isolated from WT, the double *gpsA*/*glpD* mutant (Δ *gpsA*/ Δ *glpD*), the *glpD* complement of the double mutant (Δ *gpsA*/*glpD*⁺) and the *gpsA* and *glpD* double complement of the double mutant (*gpsA*⁺/*glpD*⁺) strains, and a NTC was analyzed by PCR using primers 7 (*glpD*_1F+SacI) and 8 (*glpD*_1267R+AatII). *B. burgdorferi* strains were grown in BSK+RS at 35°C, total cell lysates were collected and equal amounts separated by SDS-PAGE; proteins were transferred to membranes and analyzed by immunoblot with antibodies against (H) GpsA (upper panel) or FlaB (lower panel) or (I) GlpD (upper panel) or FlaB (lower panel). (TIF)

S2 Fig. Sensitivity of the *gpsA* mutant to reactive oxygen species (H₂O₂). Wild-type (WT), *gpsA* mutant and *gpsA* complemented (*gpsA*⁺) strains were grown in pyruvate-free BSK + RS at 35°C to late log phase. Cultures were left untreated or treated with freshly prepared 0.2 mM H₂O₂ for 2 h at 35°C before plating in semi-solid BSK. Plates were incubated for 10–15 days at 35°C, individual colonies were enumerated and percent survival expressed as (# of colonies in 0.2 mM H₂O₂ / # colonies in untreated) × 100. Data are from three biological replicates where circles represent individual data points and the bar represents the mean. No statistical difference was observed between the mean survival of each strain as determined by one-way ANOVA with a Tukey's *post-hoc* test.

(TIF)

S3 Fig. GlpD deletion results in an opposing but less severe metabolic pattern to GpsA deletion. (A) Metabolites that significantly vary between Δ *glpD* and wild type (WT) with a false discovery rate (FDR) less than 5%. Values in the heatmap at left are displayed as the log₂(-fold change mutant versus WT) and values in the accompanying heatmap at right indicate whether that metabolite passes a 5% FDR filter for the indicated comparison as assessed by a Benjamini-Hochberg correction. (B) Metabolic map of the changes in glycolysis and the glycerol shunt that occur with the loss of GlpD. All measured metabolites in the included pathways are displayed. The log₂(fold change Δ *glpD* versus WT) is displayed as color of the node and the -log(*p*-value) is displayed as the size of the node. Enzymes in the glycerol arm of metabolism are displayed as diamonds.

(TIF)

S4 Fig. GpsA does not affect OspC and OspA protein levels. Extracts from wild-type (WT), Δ *gpsA* mutant, *gpsA* complement (*gpsA*⁺) and Δ *gpsA*/ Δ *glpD* double mutant cells grown at 35°C (without a temperature shift) were separated by SDS-PAGE and analyzed by immunoblot using antibodies against FlaB, OspC or OspA. At least three independent experiments were performed and representative image is shown.

(TIF)

Acknowledgments

We are grateful to the LAR staff for animal care in all mouse experiments. We thank Tom Schwan for anti-FlaB antibodies and Pat Secor for the pUC18 expression vector and use of the plate reader for luminescence experiments. We also thank Steve Lodmell for critical review of the manuscript.

Author Contributions

Conceptualization: Dan Drecktrah, Meghan C. Lybecker, D. Scott Samuels.

Data curation: Benjamin Schwarz.

Formal analysis: Dan Drecktrah, Laura S. Hall, Benjamin Schwarz, D. Scott Samuels.

Funding acquisition: Dan Drecktrah, Frank Gherardini, Catharine M. Bosio, Meghan C. Lybecker, D. Scott Samuels.

Investigation: Dan Drecktrah, Laura S. Hall, Bethany Crouse, Benjamin Schwarz, Crystal Richards, Eric Bohrsen, Michael Wulf, Bonnie Long, Jessica Bailey.

Methodology: Dan Drecktrah.

Project administration: Dan Drecktrah, D. Scott Samuels.

Supervision: Dan Drecktrah, Frank Gherardini, Catharine M. Bosio, D. Scott Samuels.

Visualization: Dan Drecktrah.

Writing – original draft: Dan Drecktrah, Benjamin Schwarz, D. Scott Samuels.

Writing – review & editing: Dan Drecktrah, Laura S. Hall, Bethany Crouse, Benjamin Schwarz, Crystal Richards, Eric Bohrnson, Michael Wulf, Bonnie Long, Jessica Bailey, Frank Gherardini, Catharine M. Bosio, Meghan C. Lybecker, D. Scott Samuels.

References

1. Kugeler KJ, Schwartz AM, Delorey MJ, Mead PS, Hinckley AF. Estimating the frequency of Lyme disease diagnoses, United States, 2010–2018. *Emerg Infect Dis.* 2021; 27(2):616–9. Epub 2021/01/27. <https://doi.org/10.3201/eid2702.202731> PMID: 33496229; PubMed Central PMCID: PMC7853543.
2. Burgdorfer W, Barbour AG, Hayes SF, Benach JL, Grunwaldt E, Davis JP. Lyme disease—a tick-borne spirochetosis? *Science.* 1982; 216:1317–9. <https://doi.org/10.1126/science.7043737> PMID: 7043737
3. Benach JL, Bosler EM, Hanrahan JP, Coleman JL, Bast TF, Habicht GS, et al. Spirochetes isolated from the blood of two patients with Lyme disease. *N Engl J Med.* 1983; 308:740–2. <https://doi.org/10.1056/NEJM198303313081302> PMID: 6828119
4. Steere AC, Grodzicki RL, Kornblatt AN, Craft JE, Barbour AG, Burgdorfer W, et al. The spirochetal etiology of Lyme disease. *N Engl J Med.* 1983; 308:733–40. <https://doi.org/10.1056/NEJM198303313081301> PMID: 6828118
5. Fraser CM, Casjens S, Huang WM, Sutton GG, Clayton R, Lathigra R, et al. Genomic sequence of a Lyme disease spirochete, *Borrelia burgdorferi*. *Nature.* 1997; 390:580–6. <https://doi.org/10.1038/37551> PMID: 9403685
6. Gherardini FC, Dulebohn DP, Bourret TJ, Richards CR. Metabolism and physiology of *Borrelia*. In: Radolf JD, Samuels DS, editors. *Lyme Disease and Relapsing Fever Spirochetes: Genomics, Molecular Biology, Host Interactions, and Disease Pathogenesis*. Norfolk, England: Caister Academic Press; 2021; 2021. p. 131–79.
7. Corona A, Schwartz I. *Borrelia burgdorferi*: carbon metabolism and the tick-mammal enzootic cycle. *Microbiol Spectrum.* 2015; 3(3):167–84. Epub 2015/07/18. <https://doi.org/10.1128/microbiolspec.MBP-0011-2014> PMID: 26185064.
8. Caimano MJ, Drecktrah D, Kung F, Samuels DS. Interaction of the Lyme disease spirochete with its tick vector. *Cell Microbiol.* 2016; 18(7):919–27. Epub 2016/05/06. <https://doi.org/10.1111/cmi.12609> PMID: 27147446; PubMed Central PMCID: PMC5067140.
9. von Lackum K, Stevenson B. Carbohydrate utilization by the Lyme borreliosis spirochete, *Borrelia burgdorferi*. *FEMS Microbiol Lett.* 2005; 243(1):173–9. <https://doi.org/10.1016/j.femsle.2004.12.002> PMID: 15668016.
10. Tilly K, Elias AF, Errett J, Fischer E, Iyer R, Schwartz I, et al. Genetics and regulation of chitobiose utilization in *Borrelia burgdorferi*. *J Bacteriol.* 2001; 183(19):5544–53. <https://doi.org/10.1128/JB.183.19.5544-5553.2001> PMID: 11544216.
11. Hoon-Hanks LL, Morton EA, Lybecker MC, Battisti JM, Samuels DS, Drecktrah D. *Borrelia burgdorferi malQ* mutants utilize disaccharides and traverse the enzootic cycle. *FEMS Immunol Med Microbiol.* 2012; 66(2):157–65. Epub 2012/06/08. <https://doi.org/10.1111/j.1574-695X.2012.00996.x> PMID: 22672337; PubMed Central PMCID: PMC3465622.
12. Pappas CJ, Iyer R, Petzke MM, Caimano MJ, Radolf JD, Schwartz I. *Borrelia burgdorferi* requires glycerol for maximum fitness during the tick phase of the enzootic cycle. *PLOS Pathog.* 2011; 7(7):e1002102. Epub 2011/07/14. <https://doi.org/10.1371/journal.ppat.1002102> PMID: 21750672; PubMed Central PMCID: PMC3131272.
13. He M, Ouyang Z, Troxell B, Xu H, Moh A, Piesman J, et al. Cyclic di-GMP is essential for the survival of the Lyme disease spirochete in ticks. *PLOS Pathog.* 2011; 7(6):e1002133. <https://doi.org/10.1371/journal.ppat.1002133> PMID: 21738477
14. Caimano MJ, Dunham-Ems S, Allard AM, Cassera MB, Kenedy M, Radolf JD. Cyclic di-GMP modulates gene expression in Lyme disease spirochetes at the tick-mammal interface to promote spirochete survival during the blood meal and tick-to-mammal transmission. *Infect Immun.* 2015; 83(8):3043–60. Epub 2015/05/20. <https://doi.org/10.1128/IAI.00315-15> PMID: 25987708.
15. Bugrysheva JV, Pappas CJ, Terekhova DA, Iyer R, Godfrey HP, Schwartz I, et al. Characterization of the Rel_{Bbu} regulon in *Borrelia burgdorferi* reveals modulation of glycerol metabolism by (p)ppGpp.

- PLOS One. 2015; 10(2):e0118063. Epub 2015/02/18. <https://doi.org/10.1371/journal.pone.0118063> PMID: 25688856; PubMed Central PMCID: PMC4331090.
16. Samuels DS, Lybecker MC, Yang XF, Ouyang Z, Bourret TJ, Boyle WK, et al. Gene Regulation and Transcriptomics. *Curr Issues Mol Biol*. 2021; 42:223–66. Epub 2020/12/11. <https://doi.org/10.21775/cimb.042.223> PMID: 33300497; PubMed Central PMCID: PMC7946783.
 17. Boyle WK, Groshong AM, Drecktrah D, Boylan JA, Gherardini FC, Blevins JS, et al. DksA controls the response of the Lyme disease spirochete *Borrelia burgdorferi* to starvation. *J Bacteriol*. 2019; 201(4). Epub 2018/11/28. <https://doi.org/10.1128/JB.00582-18> PMID: 30478087; PubMed Central PMCID: PMC6351744.
 18. Drecktrah D, Lybecker M, Popitsch N, Rescheneder P, Hall LS, Samuels DS. The *Borrelia burgdorferi* RelA/SpoT homolog and stringent response regulate survival in the tick vector and global gene expression during starvation. *PLOS Pathog*. 2015; 11(9):e1005160. Epub 2015/09/16. <https://doi.org/10.1371/journal.ppat.1005160> PMID: 26371761; PubMed Central PMCID: PMC4570706.
 19. Rogers EA, Terekhova D, Zhang H-M, Hovis KM, Schwartz I, Marconi RT. Rrp1, a cyclic-di-GMP-producing response regulator, is an important regulator of *Borrelia burgdorferi* core cellular functions. *Mol Microbiol*. 2009; 71(6):1551–73. Epub 2009/02/13. PMID: 19210621 [pii] <https://doi.org/10.1111/j.1365-2958.2009.06621.x> PMID: 19210621.
 20. Ojaimi C, Brooks C, Casjens S, Rosa P, Elias A, Barbour A, et al. Profiling of temperature-induced changes in *Borrelia burgdorferi* gene expression by using whole genome arrays. *Infect Immun*. 2003; 71(4):1689–705. <https://doi.org/10.1128/IAI.71.4.1689-1705.2003> PMID: 12654782.
 21. Caimano MJ, Iyer R, Eggers CH, Gonzalez C, Morton EA, Gilbert MA, et al. Analysis of the RpoS regulon in *Borrelia burgdorferi* in response to mammalian host signals provides insight into RpoS function during the enzootic cycle. *Mol Microbiol*. 2007; 65(5):1193–217. Epub 2007/07/25. PMID: 17645733 [pii] <https://doi.org/10.1111/j.1365-2958.2007.05860.x> PMID: 17645733.
 22. Miller CL, Karna SL, Seshu J. *Borrelia* host adaptation Regulator (BadR) regulates *rpoS* to modulate host adaptation and virulence factors in *Borrelia burgdorferi*. *Mol Microbiol*. 2013; 88(1):105–24. Epub 2013/02/08. <https://doi.org/10.1111/mmi.12171> PMID: 23387366; PubMed Central PMCID: PMC4828661.
 23. Zhang JJ, Chen T, Yang Y, Du J, Li H, Troxell B, et al. Positive and negative regulation of glycerol utilization by the c-di-GMP binding protein PlzA in *Borrelia burgdorferi*. *J Bacteriol*. 2018; 200(22):e00243–18. Epub 2018/09/06. <https://doi.org/10.1128/JB.00243-18> PMID: 30181123; PubMed Central PMCID: PMC6199477.
 24. Schwan TG, Battisti JM, Porcella SF, Raffel SJ, Schrupf ME, Fischer ER, et al. Glycerol-3-phosphate acquisition in spirochetes: distribution and biological activity of glycerophosphodiester phosphodiesterase (GlpQ) among *Borrelia* species. *J Bacteriol*. 2003; 185(4):1346–56. Epub 2003/02/04. <https://doi.org/10.1128/JB.185.4.1346-1356.2003> PMID: 12562805; PubMed Central PMCID: PMC142843.
 25. Bell RM. Mutants of *Escherichia coli* defective in membrane phospholipid synthesis: macromolecular synthesis in an *sn*-glycerol 3-phosphate acyltransferase K_m mutant. *J Bacteriol*. 1974; 117(3):1065–76. Epub 1974/03/01. <https://doi.org/10.1128/jb.117.3.1065-1076.1974> PubMed Central PMCID: PMC246585. PMID: 4591941
 26. Barbour AG. Isolation and cultivation of Lyme disease spirochetes. *Yale J Biol Med*. 1984; 57:521–5. PMID: 6393604
 27. Alban PS, Johnson PW, Nelson DR. Serum-starvation-induced changes in protein synthesis and morphology of *Borrelia burgdorferi*. *Microbiology*. 2000; 146:119–27. Epub 2000/02/05. <https://doi.org/10.1099/00221287-146-1-119> PMID: 10658658.
 28. Brorson Ø, Brorson SH. A rapid method for generating cystic forms of *Borrelia burgdorferi*, and their reversal to mobile spirochetes. *APMIS*. 1998; 106(12):1131–41. Epub 1999/03/03. <https://doi.org/10.1111/j.1699-0463.1998.tb00269.x> PMID: 10052721.
 29. Dunham-Ems SM, Caimano MJ, Eggers CH, Radolf JD. *Borrelia burgdorferi* requires the alternative sigma factor RpoS for dissemination within the vector during tick-to-mammal transmission. *PLOS Pathog*. 2012; 8(2):e1002532. Epub 2012/02/24. <https://doi.org/10.1371/journal.ppat.1002532> PPATHOGENS-D-11-02228 [pii]. PMID: 22359504.
 30. Green AE, Howarth D, Chaguza C, Echlin H, Langendonk RF, Munro C, et al. Pneumococcal colonization and virulence factors identified via experimental evolution in infection models. *Mol Biol Evol*. 2021; 38(6):2209–26. Epub 2021/01/28. <https://doi.org/10.1093/molbev/msab018> PMID: 33502519; PubMed Central PMCID: PMC8136498.
 31. Brunner NA, Brinkmann H, Siebers B, Hensel R. NAD⁺-dependent glyceraldehyde-3-phosphate dehydrogenase from *Thermoproteus tenax*: the first identified archaeal member of the aldehyde dehydrogenase superfamily is a glycolytic enzyme with unusual regulatory properties. *J Biol Chem*. 1998; 273(11):6149–56. Epub 1998/04/16. <https://doi.org/10.1074/jbc.273.11.6149> PMID: 9497334

32. Policastro PF, Schwan TG. Experimental infection of *Ixodes scapularis* larvae (Acari: Ixodidae) by immersion in low passage cultures of *Borrelia burgdorferi*. *J Med Entomol*. 2003; 40(3):364–70. <https://doi.org/10.1603/0022-2585-40.3.364> PMID: 12943118.
33. Liang Q, Vallance BA. What's for dinner? How *Citrobacter rodentium*'s metabolism helps it thrive in the competitive gut. *Curr Opin Microbiol*. 2021; 63:76–82. Epub 2021/07/10. <https://doi.org/10.1016/j.mib.2021.06.004> PMID: 34243134.
34. Blotz C, Stülke J. Glycerol metabolism and its implication in virulence in *Mycoplasma*. *FEMS Microbiol Rev*. 2017; 41(5):640–52. Epub 2017/09/30. <https://doi.org/10.1093/femsre/fux033> PMID: 28961963.
35. Kim M, Lee J, Heo L, Lee SJ, Han SW. Proteomic and phenotypic analyses of a putative glycerol-3-phosphate dehydrogenase required for virulence in *Acidovorax citrulli*. *Plant Pathol J*. 2021; 37(1):36–46. Epub 2021/02/09. <https://doi.org/10.5423/PPJ.OA.12.2020.0221> PMID: 33551695; PubMed Central PMCID: PMC7847757.
36. Saenz HL, Engel P, Stoeckli MC, Lanz C, Raddatz G, Vayssier-Taussat M, et al. Genomic analysis of *Bartonella* identifies type IV secretion systems as host adaptability factors. *Nat Genet*. 2007; 39(12):1469–76. Epub 2007/11/27. <https://doi.org/10.1038/ng.2007.38> PMID: 18037886.
37. Baba T, Ara T, Hasegawa M, Takai Y, Okumura Y, Baba M, et al. Construction of *Escherichia coli* K-12 in-frame, single-gene knockout mutants: the Keio collection. *Mol Syst Biol*. 2006; 2:2006 0008. Epub 2006/06/02. <https://doi.org/10.1038/msb4100050> PMID: 16738554; PubMed Central PMCID: PMC1681482.
38. Cronan JE Jr., Bell RM. Mutants of *Escherichia coli* defective in membrane phospholipid synthesis: mapping of the structural gene for L-glycerol 3-phosphate dehydrogenase. *J Bacteriol*. 1974; 118(2):598–605. Epub 1974/05/01. <https://doi.org/10.1128/jb.118.2.598-605.1974> PMID: 4597451; PubMed Central PMCID: PMC246793.
39. Fitzgerald BL, Molins CR, Islam MN, Graham B, Hove PR, Wormser GP, et al. Host metabolic response in early Lyme disease. *J Proteome Res*. 2020; 19(2):610–23. Epub 2019/12/11. <https://doi.org/10.1021/acs.jproteome.9b00470> PMID: 31821002; PubMed Central PMCID: PMC7262776.
40. Molins CR, Ashton LV, Wormser GP, Hess AM, Delorey MJ, Mahapatra S, et al. Development of a metabolic biosignature for detection of early Lyme disease. *Clin Infect Dis*. 2015; 60(12):1767–75. Epub 2015/03/13. <https://doi.org/10.1093/cid/civ185> PMID: 25761869; PubMed Central PMCID: PMC4810808.
41. Boylan JA, Hummel CS, Benoit S, Garcia-Lara J, Treglown-Downey J, Crane EJ, III, et al. *Borrelia burgdorferi* *bb0728* encodes a coenzyme A disulphide reductase whose function suggests a role in intracellular redox and the oxidative stress response. *Mol Microbiol*. 2006; 59(2):475–86. Epub 2006/01/05. <https://doi.org/10.1111/j.1365-2958.2005.04963.x> PMID: 16390443.
42. Eggers CH, Caimano MJ, Malizia RA, Kariu T, Cusack B, Desrosiers DC, et al. The coenzyme A disulphide reductase of *Borrelia burgdorferi* is important for rapid growth throughout the enzootic cycle and essential for infection of the mammalian host. *Mol Microbiol*. 2011; 82(3):679–97. Epub 2011/09/20. <https://doi.org/10.1111/j.1365-2958.2011.07845.x> PMID: 21923763; PubMed Central PMCID: PMC3226778.
43. Esteve-Gassent MD, Elliott NL, Seshu J. *sodA* is essential for virulence of *Borrelia burgdorferi* in the murine model of Lyme disease. *Mol Microbiol*. 2009; 71(3):594–612. Epub 2008/12/02. <https://doi.org/10.1111/j.1365-2958.2008.06549.x> PMID: 19040638.
44. Esteve-Gassent MD, Smith TC 2nd, Small CM, Thomas DP, Seshu J. Absence of *sodA* increases the levels of oxidation of key metabolic determinants of *Borrelia burgdorferi*. *PLOS One*. 2015; 10(8):e0136707. Epub 2015/09/01. <https://doi.org/10.1371/journal.pone.0136707> PMID: 26322513; PubMed Central PMCID: PMC4556403.
45. Brorson Ø, Brorson SH. Transformation of cystic forms of *Borrelia burgdorferi* to normal, mobile spirochetes. *Infection*. 1997; 25(4):240–6. Epub 1997/07/01. <https://doi.org/10.1007/BF01713153> PMID: 9266264.
46. Boylan JA, Lawrence KA, Downey JS, Gherardini FC. *Borrelia burgdorferi* membranes are the primary targets of reactive oxygen species. *Mol Microbiol*. 2008; 68(3):786–99. Epub 2008/04/01. <https://doi.org/10.1111/j.1365-2958.2008.06204.x> PMID: 18373524; PubMed Central PMCID: PMC2327290.
47. Li X, Pal U, Ramamoorthi N, Liu X, Desrosiers DC, Eggers CH, et al. The Lyme disease agent *Borrelia burgdorferi* requires BB0690, a Dps homologue, to persist within ticks. *Mol Microbiol*. 2007; 63(3):694–710. Epub 2006/12/22. <https://doi.org/10.1111/j.1365-2958.2006.05550.x> PMID: 17181780.
48. Iyer R, Caimano MJ, Luthra A, Axline D Jr., Corona A, Iacobas DA, et al. Stage-specific global alterations in the transcriptomes of Lyme disease spirochetes during tick feeding and following mammalian host adaptation. *Mol Microbiol*. 2015; 95(3):509–38. Epub 2014/11/27. <https://doi.org/10.1111/mmi.12882> PMID: 25425211.

49. Purser JE, Norris SJ. Correlation between plasmid content and infectivity in *Borrelia burgdorferi*. *Proc Natl Acad Sci USA*. 2000; 97(25):13865–70. <https://doi.org/10.1073/pnas.97.25.13865> PMID: [11106398](https://pubmed.ncbi.nlm.nih.gov/11106398/).
50. Samuels DS, Drecktrah D, Hall LS. Genetic transformation and complementation. In: Pal U, Buyuktanir O, editors. *Borrelia burgdorferi*: Methods and Protocols. 1690. 2017/10/17 ed. New York, NY: Humana Press; 2018. p. 183–200.
51. Bertani G. Studies on lysogenesis: I. The mode of phage liberation by lysogenic *Escherichia coli*. *J Bacteriol*. 1951; 62(3):293–300. Epub 1951/09/01. <https://doi.org/10.1128/jb.62.3.293-300.1951> PMID: [14888646](https://pubmed.ncbi.nlm.nih.gov/14888646/).
52. Frank KL, Bundle SF, Kresge ME, Eggers CH, Samuels DS. *aadA* confers streptomycin-resistance in *Borrelia burgdorferi*. *J Bacteriol*. 2003; 185(22):6723–7. <https://doi.org/10.1128/JB.185.22.6723-6727.2003> PMID: [14594849](https://pubmed.ncbi.nlm.nih.gov/14594849/).
53. Babitzke P, Yealy J, Campanelli D. Interaction of the *trp* RNA-binding attenuation protein (TRAP) of *Bacillus subtilis* with RNA: effects of the number of GAG repeats, the nucleotides separating adjacent repeats, and RNA secondary structure. *J Bacteriol*. 1996; 178(17):5159–63. Epub 1996/09/01. <https://doi.org/10.1128/jb.178.17.5159-5163.1996> PMID: [8752333](https://pubmed.ncbi.nlm.nih.gov/8752333/); PubMed Central PMCID: PMC178312.
54. Yang XF, Pal U, Alani SM, Fikrig E, Norgard MV. Essential role for OspA/B in the life cycle of the Lyme disease spirochete. *J Exp Med*. 2004; 199(5):641–8. <https://doi.org/10.1084/jem.20031960> PMID: [14981112](https://pubmed.ncbi.nlm.nih.gov/14981112/).
55. Bunikis I, Kutschan-Bunikis S, Bonde M, Bergström S. Multiplex PCR as a tool for validating plasmid content of *Borrelia burgdorferi*. *J Microbiol Methods*. 2011; 86(2):243–7. Epub 2011/05/25. <https://doi.org/10.1016/j.mimet.2011.05.004> PMID: [21605603](https://pubmed.ncbi.nlm.nih.gov/21605603/).
56. McCloskey D, Gangoiti JA, Palsson BO, Feist AM. A pH and solvent optimized reverse-phase ion-pairing-LC-MS/MS method that leverages multiple scan-types for targeted absolute quantification of intracellular metabolites. *Metabolomics*. 2015; 11:1338–50.
57. Schwarz B, Sharma L, Roberts L, Peng X, Bermejo S, Leighton I, et al. Severe SARS-CoV-2 infection in humans is defined by a shift in the serum lipidome, resulting in dysregulation of eicosanoid immune mediators. *J Immunol*. 2021; 206(2):329–34. Epub 2020/12/06. <https://doi.org/10.4049/jimmunol.2001025> PMID: [33277388](https://pubmed.ncbi.nlm.nih.gov/33277388/); PubMed Central PMCID: PMC7962598.